Detection of Damage Precursors in Steel Components for Life-Cycle Assessment

FINAL REPORT
October 2019

Submitted by

Sophia Hassiotis Ph.D.
Associate Professor, CE
Stevens Institute of Technology
Hoboken, N.J. 07030

Dimitri Donskoy Ph.D.
Associate Professor, CE
Stevens Institute of Technology
Hoboken, N.J. 07030

Marcus Rutner Ph.D.
Associate Professor, CE
TUHH
Hamburg, Germany

Majid Ramezani Goldyani
Ph.D. Candidate
Stevens Institute of Technology
Hoboken, N.J. 07030

Behnoush Golchinfar
Ph.D. Candidate
Stevens Institute of Technology
Hoboken, N.J. 07030

NJDOT Research Project Manager
Giri Venkiteela, Ph.D.

In cooperation with

New Jersey
Department of Transportation
Bureau of Research
And
U. S. Department of Transportation
Federal Highway Administration

1. Report No. FHWA NJ-20XX-0XX	2.Government Accession No.	3. Recipient's Catalog No.
4. Title and Subtitle FINAL REPORT Detection of Damage Precursors in Steel Components for Life-Cycle Assessments		5. Report Date **October 2019**
		6. Performing Organization Code Stevens Institute of Technology
7. Author(s) Hassiotis, Sophia Ph.D. and Donskoy, Dimitri Ph.D.		8. Performing Organization Report No.
9. Performing Organization Name and Address Stevens Institute of Technology Hoboken, N.J.		10. Work Unit No.
		11. Contract or Grant No. 2016-09
12. Sponsoring Agency Name and Address New Jersey Department of Transportation PO 600 Trenton, NJ 08625	Federal Highway Administration U.S. Department of Transportation Washington, D.C. 20590	13. Type of Report and Period Covered Final Submission October, 2019
		14. Sponsoring Agency Code NJDOT, FHWA
15. Supplementary Notes		

16. Abstract

The early identification of damage of fracture-critical members is of the outmost importance in the maintenance of a safe bridge infrastructure. A new Non-Destructive Evaluation method that gives an early warning of accumulating damage is been formulated herein. The Vibro-Acoustic Modulation method utilizes nonlinear interactions of a high frequency ultrasonic wave with a low frequency modulating vibration in the presence of various flaws such as fatigue and stress-corrosion cracks. The growth of a flaw in time is correlated with with an increase in a parameter called the Modulation Index which is defined in the spectral domain as the ratio of the side-band spectral components formed at frequencies around the amplitude of the carrier. The new method is shown capable of detecting damage in simple during cyclic loading. An experimental set-up has been fabricated that can be taken to the field for farther developments of the new NDE method.

17. Key Words Vibro-Acoustic Modulation, Acoustic Methods, Damage Detection, Fatigue, Fracture	18. Distribution Statement		
19. Security Classif (of this report) Unclassified	20. Security Classif. (of this page) Unclassified	21. No of Pages	22. Price

Form DOT F 1700.7 (8-69)

ACKNOWLEDGEMENTS

TABLE OF CONTENTS

Page

LIST OF FIGURES

Page

LIST OF TABLES

Page

EXECUTIVE SUMMARY

The main reason for the failure of metallic structures is crack propagation. Up to 90 percent of failures of in-service metallic structures happen due to fatigue cracks. A fatigue crack is initiated from a damage precursor at unperceivable level (e.g. dislocation or micro crack in materials) when the material is subjected to repeated loading. The precursor can often continue to grow to a critical point without sufficient warning, leading to catastrophic consequences.

Continuous monitoring of structures and large sensing level of ultrasonic techniques, among other nondestructive testing and structural health monitoring techniques, facilitate the online monitoring of fatigue cracks. Traditional active acoustic/ultrasonic methods are not sensitive enough to fatigue cracks until they become completely visible because these techniques use the linear properties of scattering, transmission, reflection and attenuation of the elastic waves to detect damages. These methods have inherent limitations. For example, traditional ultrasonic techniques are not capable of detecting initial damages of a size smaller than wavelength of the transmitted wave. Another disadvantage is distinguishing between the actual damage versus structural features of comparable or greater size, such as notches, holes, borders, and other structural features. Reflections of these structural features mask the signal relating to the damage. One possible approach to tackle these limitations is to explore the nonlinear nature of the material damage by utilizing nonlinear acoustic methods for damage detection.

Nonlinear Vibro-Acoustic Modulation is one of the prevailing nonlinear methods for material characterization and structural-damage evaluation. This approach, however, does not differentiate between the amplitude and frequency modulations. The present study aims to develop algorithms that separate the two modulations. It is shown that the commonly used Hilbert Transform separation does not work well for a typical Vibro-Acoustic Modulation scenario. By separating the amplitude and frequency modulations, the algorithms developed herein address shortcomings of the Hilbert Transform and contribute to an improved non-linear acoustic method for damage detection. The algorithms have been tested both numerically and experimentally for their ability to detect the evolution of fatigue damage in the presence of additional nonlinearities provided by bolts, welding, or corrosion.

The new algorithms have been incorporated into an N-Scan testing system that will be employable for field-testing in order to enhance its capabilities to detect damage in large-scale and full-scale structures.

BACKGROUND

Heavy cyclic loads exerted on steel components of bridges lead to fatigue degradation of structural material which may finally trigger an irreversible fracture process. The phenomena of fatigue fracture and ultimate loss of structural integrity depend on a) loading characteristics, which include the frequency spectra, maximum stress and strain ratio, b) environmental conditions, such as temperature, or aggressive environment, and c) material properties, such as chemical makeup, morphology (grain size, grain structure, and grain boundaries), or type and spatial distribution of microdefects resulting from material and manufacturing conditions of structural components.
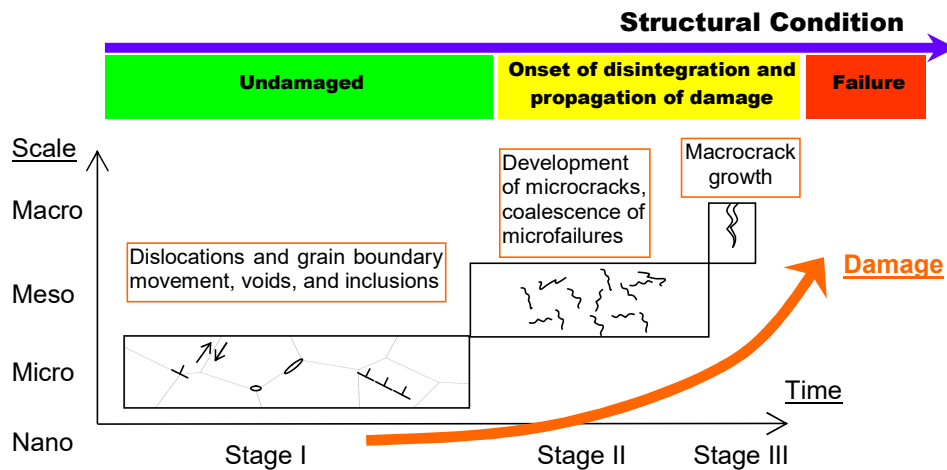
Figure 1. Damage accumulation and growth diagram

Three stages of the fracture process are shown schematically in Figure 1.[1] The first stage is the damage accumulation stage, which consists of nucleation and growth of sub-micro- and micro-defects within the individual grain and grain boundaries. This stage, also called an incubation period of fracture, ends by interaction and coalescence of the micro-defects resulting in small crack formation (a "small" crack from continuum mechanics view point should not be smaller than about ten grain size). In most practical situations, it is assumed that sub-micro and micro imperfections developed at the first damage accumulation stage have very little or no effect on structural performance and, thus, structure is considered being "healthy". Individual micro-crack growth constitutes the second stage of fracture process. After certain time of micro-crack growth, the initially small cracks reach proximity of one another and start to interact. The crack size, at which the interaction begins, depends on density and spatial distribution of micro-cracks formed at the end of the incubation period. Further growth of strongly interacting micro-cracks and formation of clusters of micro-cracks constitutes the third stage of fracture process. At this stage the clusters evolution leads to a dynamic growth of one or a few macro-cracks resulting in the ultimate failure. The third stage of the process is relatively short in comparison with first two stages. The total lifetime of a structural component is approximately a sum of the duration of the first and the second stages of fatigue fracture as it is illustrated Figure 1. When the evidence of the third stage is

found, the component must be replaced in order to prevent fatal consequences. In other words, at the third stage, it is already clear that the component is inoperable and no prediction of the remaining life is needed. While it is essential that the third stage of the fracture process be detected timely, it is even more important to evaluate structural condition at the preceding stages. This could be accomplished using a nondestructive inspection technique, which is capable of monitoring structural health at meso- and micro- scales, i.e. before fracture.

Current specifications enforce bridge inspections to guarantee the safety of bridge infrastructure. The bridge inspections today consist mainly of visual field inspection of each bridge element and the recording of the number and severity of the defects.[2] The NJDOT Bridge Elements Inspection Manual[3] adopted the guidelines for the element inspection of its inventory. Transportation engineers use bridge management software that provides the means to store the bridge element inspection data, track preservation and maintenance, perform deterioration modeling, and guide toward the most cost-effective choices for bridge rehabilitation and replacement. Guidance on the evaluation of steel bridges for fatigue can be found AASHTO specifications[4,5,6] and Bridge Evaluations Manuals.[7] A recently published NCHRP report summarizes the latest developments on the subject.[7] The current methodology as defined in the AASHTO Manuals applied for the fatigue assessment of bridge components is based on constructing the accumulated damage index according to Palmgren-Miner rule and based on the S-N curves. Applying the S-N curve for life-cycle assessment of a specific bridge component involves extensive measurements, such as traffic volume, loading and cyclic stress range in the component. Further, using the S-N curves (A to E') in the fatigue assessment leads in some cases to rather conservative results.[8]

Bridges may comprise fracture critical members (FCM). Eleven per-cent of the steel bridges in the United States have FCMs, and approximately 76% of the FCMs were fabricated before 1978.[9] As such, "Hands-on" fracture-critical inspection is mandated since 1988 by the FHWA's National Bridge Inspection Standards.

The National Bridge Inspection Standards were mandated after the study of collapse and catastrophic failures of bridges due to fracture. In 1967, the Silver Bridge over the Ohio River at Point Pleasant, West Virginia collapsed due to a brittle fracture caused by stress-corrosion cracking. It was the collapse of this bridge that initiated a national bridge inspection program that resulted in many changes in material, design, and inspection of steel bridges.[9] In 1983, failure of the Mianus River Bridge in Connecticut further alerted the community to the vulnerability of the FCM bridges and resulted in mandated inspections. Such cracking should not be possible in modern bridge steel, but many older bridges are still in use and are vulnerable. For example, the Interstate 5 Bridge over the Skagit River which collapsed in 2013 was a fracture-critical bridge.

A partial list of fracture-critical load-carrying members in need of visual inspection includes steel elements such as: 1) girders, beams, floor-beams and stringers 2) tension members of trusses 3) box girders 4) main suspension cables 5) hangers of suspension or arch bridges 6) ties of arches or trusses 7) pin-and-hanger assemblies.

A Fracture critical bridge inspection is defined as a "hands-on" inspection by the FHWA-National Bridge Inspection Standards. That is, a detailed, visual, hands-on inspection is

the primary technique for detecting cracks in tension members. Other non-destructive methods are also used, such as Acoustic emissions, corrosion sensors, smart coating, dye penetrant, radiographic testing, computed tomography, robotic inspection, ultrasonic testing, eddy current etc. Nevertheless, the need for more research and development in the area has been identified.

A recent NIST Workshop on Quantitative Tools for Condition Assessment of Aging Infrastructure undertakes a critical review of urgent research topics for improved condition assessment of aging infrastructure and presents a ranking of the most urgent research topics.[10] The most urgent topic of the list of 23 topics selected by academics and bridge owners is sensor development for damage detection and measurements and quantification of structural degradation beyond visual inspection [NIST workshop manual; pp 29-30]. However, there exist only a few technologies for defect detection and their operability is severely limited. The NCHRP 354 indicates as the two most urgent and immediate research demands; a) to develop advanced fatigue-life calculation procedures taking into account the lack of visible cracks for fracture critical bridges (FCBs) and b) field monitoring for FCBs.[9]

Currently available Non-Destructive Evaluation (NDE) is limited in measuring micro-structural changes and micro flaws, so called *damage precursors*, in the material and providing a practical and efficient approach for field measurements. However, the methodology recently developed by Donskoy for US Navy[10,11] introduces a transformative effective damage assessment across length scales, i.e. of micro-sized defects as well as large cracks, and their related crack growth rate. The outcome of the damage assessment is a unit less damage index, *DI*, which represents the damage state of a structural component/member and is directly related to fatigue life. The proposed efforts will adopt this *DI* methodology for bridge structural components, and provide direct validation to procedures implemented in the AASHTO manuals. The *DI* is found by 1) placing one sensor/transducer pair anywhere on the steel structural component to pick up damage within the entire component (*including hidden spaces*) and 2) making a single measurement per critical component during every bridge inspection. The information obtained by these measurements will provide an accurate assessment of damage progression.

Accordingly, this research seeks to accomplish the following: develop a robust, large-coverage damage detection methodology capable of detecting micro-scale defects (which are not recognizable through visual inspection) as well as large cracks in complex-geometry steel infrastructure, providing information on relating damage accumulation.

OBJECTIVES

The motivation for this research is the lack of a single methodology for detection of damage precursors on the surface or in metal structural components within efficient large-area scanning, which combines the critical attributes of accuracy, efficiency, cost-effectiveness and overall robustness. The objective of this research is to develop a damage precursor sensing and monitoring technique using non-linear acoustics to be used for NDE of steel bridges. The new technique provides the following advantages compared to other monitoring technologies:

- Detection and measurement of a damage precursor, i.e. micro-size defect
- Monitoring of crack growth rate over large length scale range, i.e. from micro-sized flaws to large-sized crack
- Representation of damage with a damage index DI
- Large coverage sensing of defects by placing only one sensor/transducer pair on the structural component
- Easily applicable measurement, ensuring cost-saving, time-effective inspection
- Building a testing prototype that can be extendable into real time monitoring
- Validating existing fatigue/fracture assessment methodologies based on the S-N curves, the accumulated damage index after Palmgren-Miner, the fatigue serviceability index and the Paris law

INTRODUCTION

The use of non-linear acoustics has been found to be a strong viable method in the identification of damage. In damaged materials, the nonlinear response is attributed to strongly-nonlinear local-vibrations of defects which generate multiple ultra-harmonics and support multi-wave interactions.

Non-linearities can be produced by several mechanisms. Contact interfaces created by cracks, delamination, or de-bonding show strong nonlinearities due to clapping.[10,11,12,13] Consider a pre-stressed crack (Figure 2) which is strong enough to provide clapping of the crack interface.
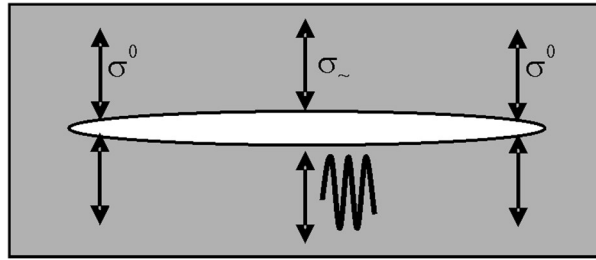
Figure 2. Model of a clapping crack[12]

The clapping nonlinearity is due to asymmetrical dynamics of the contact stiffness which is higher in compression than in tension. Other non-linearities, attributed to dislocation, friction, stress concentration and temperature gradient at the crack area, can also produce nonlinear modulation at a very low strain level without crack opening and closing.[14,15] In addition, increased nonlinearity is produced by fatigue damage accumulation due to dislocations, hysteresis, formation of slip planes, and development and clustering of microcracks.[16,17,18]

The sensitivity of the nonlinear acoustic techniques (NAT) to defects has been shown to be far better than that of the linear ones.[19] In addition, nonlinear techniques can be used to detect flaws in highly inhomogeneous and complicated geometries. The main limitation of the NATs in their implementation into Non-Destructive Evaluation (NDE) is the need to establish a reference in order to separate the evolution of damage from other sources of non-linear behavior such as supports, connections, background readouts, etc. For example, the background nonlinearity must be recorded for a reference structure and a particular measurement- setup and then compared with the structure undergoing NDT. This drawback is, perhaps, one of the primary reasons that the nonlinear methods most reported are still experimental and are not yet established as practical and reliable defect detection tools.[20]

The objective of this research is to take advantage of the information carried by the non-linear acoustic data and use it to develop a viable NDE technique. In what follows, a stronger NDE method is presented that addresses some of the previously identified shortcomings.

SUMMARY OF THE LITERATURE REVIEW

Among the number of different nonlinear methods, there are two methods viable and broadly used: harmonic distortion and modulation methods. A simplified graphical illustration of these two methods is presented in Figure 3.

Harmonic Distortion Methods

Historically, one of the first methods to characterize the acoustic nonlinearity is to measure the degree of the nonlinear (harmonic) distortion of a sinusoidal acoustic (vibration) signal.
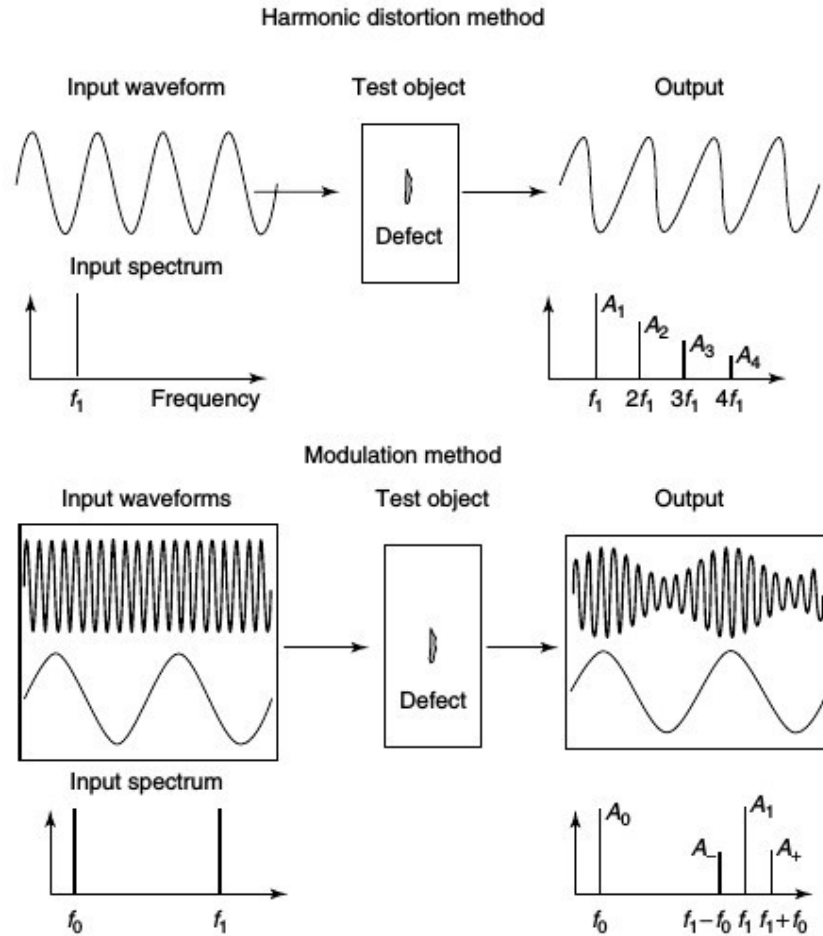
Figure 3. Illustrative diagrams of harmonic distortion and modulation methods[20]

This approach has been widely used for the characterization of nonlinearity in fluids,[21] biological media,[22,23] electromechanical systems,[24] and material nonlinearity of solids.[25-28] The essence of the method is illustrated in Figure 3. An input signal is a sinusoidal waveform with frequency f_1 and amplitude A_1. The nonlinearity distorts the waveform so its spectrum contains additional harmonics. Typically, these are higher harmonics with frequencies $2f_1, 3f_1, \cdots$ and, respectively, diminishing amplitudes $A_1 > A_2 >$

$A_3 > \cdots$. Because of this decrease in amplitude, most of the studies consider only the second harmonic for characterization of nonlinearity of defect. The second-harmonic approach has been used for evaluation of fatigue cracks,[29] dislocations and other fatigue damages.[18,30] The range of frequencies and type of acoustic/vibration waves vary significantly depending on the specific applications: type of material, size of structure, and type and size of flaws. Thus, the reported frequencies used for the nonlinear detection span from hundreds of hertz to tens of megahertz. Flexural and torsional vibrations, longitudinal, shear, surface and guided acoustic waves were utilized.[26,31]

The challenges in harmonic measurement method are system nonlinearities from electronic and electromechanical equipment, such as signal generators, amplifiers, and transducers. These signals generate a certain level of the harmonic distortion in the first place. This background level in the nonlinear signal limits the sensitivity of the method to defects with smaller nonlinearities.

Modulation Methods

The modulation methods utilize the effect of the nonlinear interaction of acoustic/vibration waves in the presence of the nonlinear defects. The instantaneous amplitude and phase were analyzed in the literature.[32,33] One study declared that the intensity of amplitude modulation corresponds better with crack lengths than the intensity of frequency modulations.[32] A similar result displayed that elevated amplitude modulation effects are measured at the damaged area, whereas there is no direct relation between the frequency modulation and the location of the damage.[33]

There are two modifications of the modulation method: Vibro-Acoustic-Modulation (VAM) and impact modulation (IM). The VAM method uses two sinusoidal waves with the frequencies f_0 and f_1. The nonlinearity of the defect causes mixing of these two signals which leads to a new signal with the combination frequencies $f_1 \pm f_0$. Typically, the VAM method exploits lower frequency modulating and higher frequency probing signals: $f_0 \ll f_1$.[11, 34, 35] Applied lower frequency vibration changes the contact area within a defect or damaged area, effectively modulating the amplitude of the higher frequency probing wave passing through the changing contacts.

In the frequency domain, this modulation manifests itself as the sideband spectral components, $f_1 \pm f_0$, as shown in Figures 4(a) and 4(b). The defect or damage can be detected and characterized by the amplitude of the sideband components or, better, the modulation index (MI) (in decibel scale):

$$MI = 20 \log_{10} \left(\frac{A_- + A_+}{2} \right) - 20 \log_{10} A_1 \tag{1}$$

Strong defect nonlinearities may lead to the occurrence of numerous sideband components with the frequencies $f_1 \pm m f_0$, where m = 1, 2, $\cdots$ as evident from Figure 4(b) and other experimental observations.[11] In practice, however, only the first

sidebands (m = 1) are used as a reliable indicator of the damage.
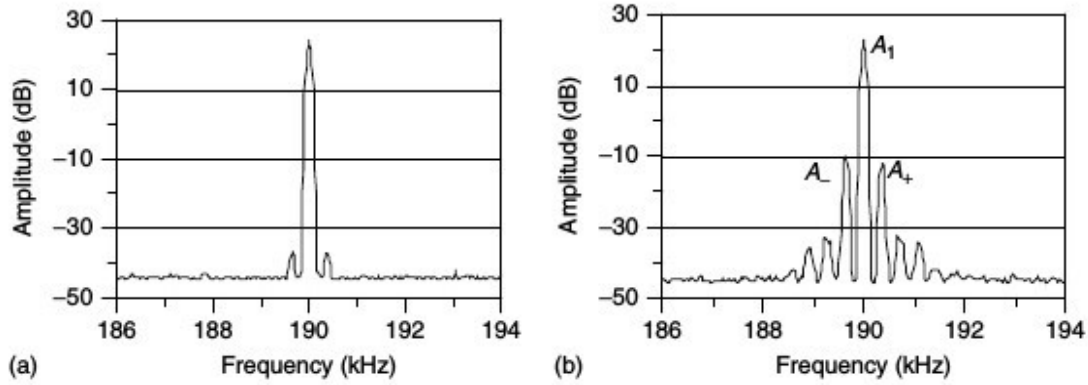
Figure 4. Spectra of a high-frequency ultrasonic signal modulated by a low frequency vibration: (a) undamaged section of the steel pipe and (b) the same pipe section with stress-corrosion cracks[11]

The main advantage of IM over the VAM approach is the ease of excitation of the low-frequency signal: a simple hammer can be used instead of an electronically controlled low-frequency vibration/acoustic source; however, IM does not work for structures with low vibration damping since modulation does not happen due to damping of low-frequency signal.

The modulation methods could be implemented using a continuous wave (CW) or a sequence of burst ultrasonic signals.[36] CW implementations of the VAM (CW-VAM) and IM (CW-IM) methods showed that the choice of the ultrasonic frequency, f_1, may have a significant impact on the MI, often leading to the erroneous interpretation of the test result. As seen from the recorded structural frequency responses of the probing ultrasonic signal and its side-bands (Figure 5), MI could vary as much as 40 dB depending on the choice of the primary frequency, f_1. This variation is because of resonances and anti-resonances of the structure. Theoretical studies[11] and numerous tests with different structures and materials[37] determined that reliable damage detection and characterization could be accomplished with frequency averaging as follows:

$$MI = 20\log_{10}(\frac{1}{N}\sum_{n=1}^{N}(\frac{A_+(f_n+f_0)+A_-(f_n-f_0)}{2A_1(f_n)}))$$ (2)

where $f_n = F_{start} + n \cdot \Delta F$ is the fundamental ultrasonic frequency swept in steps n over the frequency range $F_{start} + N \cdot \Delta F$, with F_{start} being the starting frequency, ΔF the frequency step, and N the total number of steps. In this figure, the lower two curves are the corresponding frequency responses of the sidebands $A_\pm(f_\pm)$ (also in decibel scale) at the frequencies $f_\pm = f_1 \pm 250 Hz$ recorded as f_1 is swept. MI is the modulation index (in decibels). It is graphically defined as a difference between the linearly averaged value of two lower curves and the upper curve. MI can vary as much 40 dB ($MI_1 - MI_2$) because of resonances and anti-resonances of the frequency response.[20]

The choice of ΔF is determined by the density of the resonances in the frequency response of the particular structure for the chosen frequency range. For proper averaging, ΔF should be less than the frequency separations between the resonances. The number of frequency steps should be at least 30, preferably 100. In the burst implementation of the vibro-modulation method (B-VM), a sufficiently long sequence of bursts with the central frequency f_n for each burst and the repetition frequency $F_R > 2f_0$ could be used instead of a CW ultrasonic signal. The B-VM method is more complicated to implement, requiring elaborate signal collection and processing.
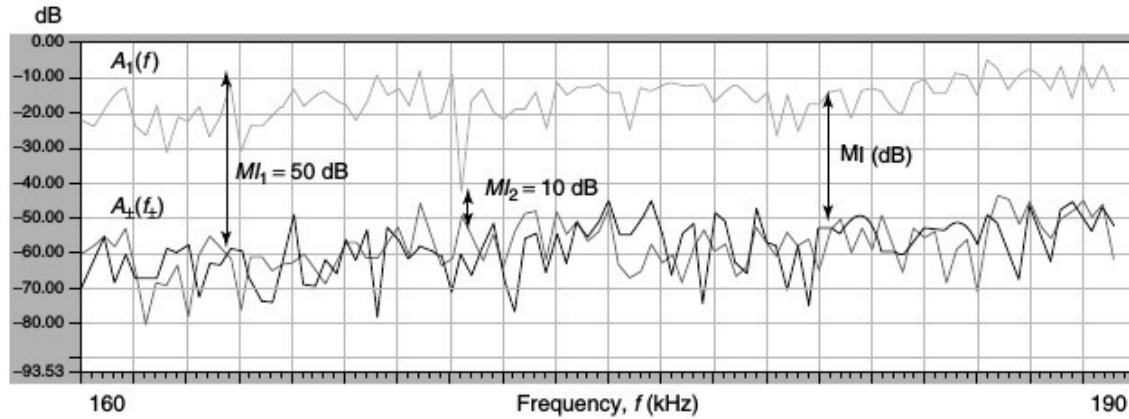
Figure 5. Frequency response ($A_1(f)$ upper curve, in decibels) of 0.5-m-long steel beam for the high-frequency ultrasonic signal f_1 swept the 160-190 kHz frequency range

One of the problems using VAM and, especially IM methods, for NDT screening for damage in multiple parts of the same kind is the calibration of the modulating vibration. On the other hand, VAM techniques can utilize vibrations of the structure during its normal operation as a modulating signal. For example, VAM monitoring of a bridge could utilize vibration due to traffic and wind, etc.

Recent research has also been performed on broadening the capabilities of VAM to localize and assess the range of damage. This research includes the use of noncontact ultrasonic transducers to localize simulated and impact damage in a thin-polystyrene plate[38] or fatigue cracks in aluminum components.[39] In both cases, the localization of damage can be achieved by scanning a certain area of the structure and mapping the intensity of modulation derived from the amplitudes of the sideband components. Similar methods are presented to localize damage detection using hybrid contact-noncontact transducers.[40,41] An approach using the combination of contact and noncontact ultrasonic transducers has also been exhibited to detect delamination in a carbon fiber reinforced laminate.[41] A photoacoustic excitation of an HF probe is has been studied.[41] The test sample is excited with vibration signals generated using a fixed piezoelectric transducer and a moving intensity–modulated laser source. Signals for the mixed frequency components are acquired by a moving accelerometer.

10

An ultrasonic method providing for an efficient global detection of defects in complex media (multiple scattering or reverberating media) has been published.[42] Mixing of coda waves (stemming from multiple scattering) with lower frequency swept vibration waves has been used to detect the damage. Coda waves are correlated with effective nonlinear parameters of the medium. Nonlinear scatterers, such as cracks and delamination lead to this nonlinear mixing step; however, this mixing is not observable when the waves are scattered only by linear scatterers, as is the case in a complex but defect-free medium. By comparing results at two damage levels, the effective nonlinear parameters are shown to be correlated with crack presence in glass samples.

In another effort, reported an all-optical probing method has been reported for the study of the nonlinear acoustics of cracks in solids.[43,44] The absorption of radiation from a pair of laser beams intensity modulated at two different frequencies initiated nonlinear acoustic waves. The detection of acoustic waves at mixed frequencies, absent in the frequency spectrum of the heating lasers, by optical interferometry or deflectometry gives obvious evidence of the elastic non-linearity of the crack. The highest acoustic nonlinearity is observed in the transitional state of the crack, which is intermediate between the open and the closed ones.

In summary, the sensitivity of linear ultrasonic testing (UT) significantly decreases as the damage size gets smaller. Being orders of magnitude more sensitive to micro- and mesoscopic damages,[17,18] nonlinear acoustics offers a unique opportunity to monitor and characterize the damage accumulation at these scales.

To confirm that the nonlinear acoustic damage index is responsive to the micro- and mesoscale structural changes, a microscopic analysis of the fatigue samples using a scanning acoustic microscope (SAM) and a scanning electron microscope (SEM) can be conducted. Investigations of the nonlinear dynamics of materials with contact-type macrodefects (cracks, disbonds, delaminations) as well as fatigued materials with micro- and mesoscale damages show their unusually high acoustic nonlinearities, often orders of magnitude greater than found in undamaged materials.

Advantages of the Nonlinear Acoustic Testing (NAT) include much higher nonlinear response contrast between damaged/undamaged materials: studies report large percentage change in the nonlinear response versus only a fraction of a percent in the linear response for the same damage. Being responsive to only nonlinear defects, the NAT can be used in structures with complicated geometries in which multiple reflections (reverberation) often preclude the use of the linear Ultrasonic Technique.

One of the difficulties in implementing NAT for many NDT applications is the requirement for a well-established "nonlinear background" reference for a particular structure. However, because SHM detects (monitors) changes in the materials/structure

over time, the initial measurements could be used as a reference for the very same structure. This reference, correlated with the extremely high responsiveness to changes due to damage, makes the NAT highly suitable for Structural Health Monitoring (SHM) applications. Additionally, many applications of the NAT are perfectly suited for monitoring of large portions of a structure using just a few sensors in fixed locations not requiring sensor spatial scanning. These advantages are the primary reasons for selecting NAT over competing techniques in some SHM applications.

SUMMARY OF THE WORK PERFORMED

The main thrust of the research that leads to a break-through in the use of non-linear acoustics to determine damage is the separation of the amplitude and phase modulations. Overall, this section is summarizing 1) original work in the development of algorithms to identify damage using non-linear acoustic measurements, 2) experimental tests on fatigue fracture to validate the algorithms, 3) experimental tests on fatigue fracture to determine the effects of stress-level, corrosion, welding and material thickness in identifying damage, 3) comparison of the VAM technique with other NDE methods, and 4) the presentation of a testing set-up to be validated for field testing.

Separation of Amplitude and Frequency Modulations in VAM

Two new algorithms: 1) In-Phase/Quadrature Homodyne Separation **(IQHS)** and 2) Sweeping-Phase Homodyne Separation **(SPHS)** have been developed for separating the amplitude and frequency modulated components of the received signal.

The VAM method utilizes nonlinear interaction of a high frequency ultrasonic wave (carrier signal) with frequency ω and a low frequency modulating vibration with frequency $\Omega << \omega$, in the presence of various flaws such as fatigue and stress-corrosion cracks, disbonds, etc. Most of the reported VAM studies correlate flaw presence and growth with the increase in the Modulation Index (MI) defined in the spectral domain as the ratio of the side-band spectral components at frequencies $\omega\pm\Omega$ to the amplitude of the carrier. This approach, however, does not differentiate between amplitude, AM, or frequency, FM, modulations contributing to the MI. It has been assumed that the prevailing modulation is AM due to contact-type nonlinear mechanisms. However, there could be other mechanisms leading to phase/frequency modulation. The present study aims to develop an algorithm of AM/FM separation specifically for the VAM method. It is shown that the commonly used Hilbert Transform (HT) separation may not work for a typical VAM scenario. The developed In-phase/Quadrature Homodyne Separation algorithm addresses HT shortcomings. The algorithm has been tested both numerically and experimentally (for fatigue crack evolution) showing FM dominance at initial micro-crack growth stages and transition to AM dominance during macro-crack formation.

AM/FM separation is not a new problem and has been extensively studied in communication and broadcasting fields where the major challenge is broadband and non-stationary nature of the modulation signals. VAM utilizes stationary harmonic modulation. For this simple modulation, the Hilbert Transform and its modifications,[45]

12

are routinely used to extract the instantaneous amplitude and phase/frequency. When this approach was attempted for AM/FM decomposition in VAM signals,[46,47] dominant AM modulation for visible cracks over 11 mm in length was reported. The data for FM modulation was inconclusive. This is not surprising, as HT separation approach may easily yield erroneous results due to a number of factors depending on nondestructive testing scenarios. First, there are amplitude and phase distortions of the modulated signal due to the structure under test (SUT) frequency transfer functions as illustrated in Figure 6.
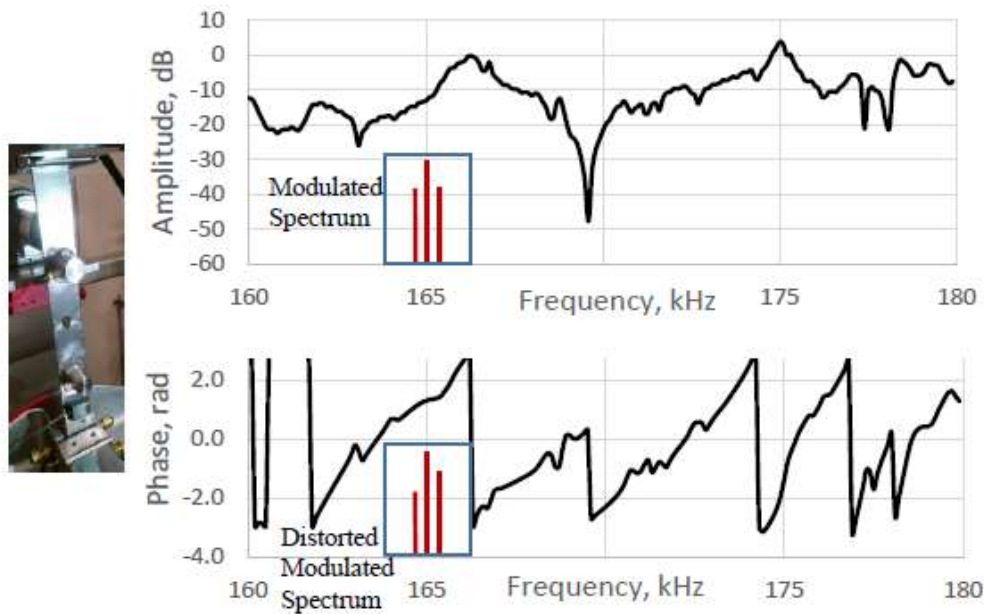
Figure 6. Illustration of the amplitude and phase distortions of the modulated signal by a sample's(picture of the left) amplitude and phase (top and bottom spectra, respectively) transfer functions

Even small distortions of amplitude and especially phase of the modulated signal spectral components will lead to significant error during the HT separation process as our extensive MATLAB simulation has demonstrated. Therefore, a procedure should be implemented to measure the SUT frequency transfer functions (TS) and to choose carrier and modulating frequencies with minimal distortion by TS or to compensate for such a distortion. This is an important step in any attempted AM/FM separation. There are other situations which will render HT separation totally incorrect. One of the common scenarios is a multipath propagation of the carrier signal such that one of the paths is passing through the defect and modulated, while the other paths are unmodulated. Because of the use of long duration carrier signal (to be able to capture and resolve the low frequency modulation), both modulated and unmodulated signals are mixed at the receiver, again making erroneous HT-based modulation decomposition.

In-phase/Quadrature Homodyne Separation (IQHS) Algorithm

In order to address the multipath-mixing problem, a new algorithm has been developed and tested both numerically and experimentally. This algorithm utilizes AM and FM reconstruction Eq.(1),[48] based on phases and amplitudes of the modulated signal spectral components, Figure 7.
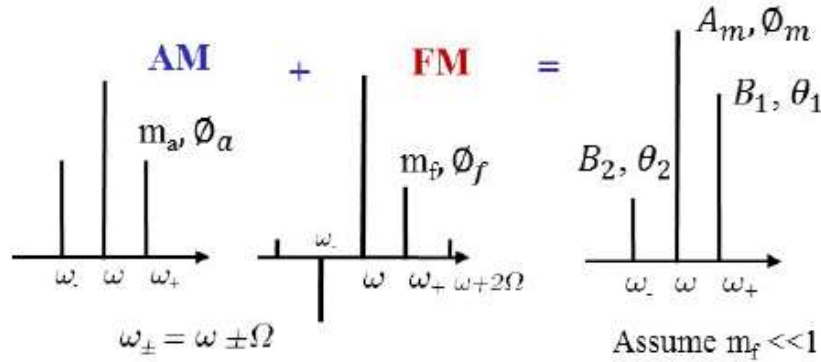
Figure 7. Spectral amplitudes and phases of the modulated signal

$$2m_a = \sqrt{B_1^2 + B_2^2 + 2B_1B_2 \cos(\theta_2 + \theta_1)} \ , \ 2m_f = \sqrt{B_1^2 + B_2^2 - 2B_1B_2 \cos(\theta_2 + \theta_1)} \quad (3)$$

Here the accurate determination of $\theta_1 + \theta_2$ is the key for correct separation of the modulations. In these notations pure AM is taking place if $\theta_1 = -\theta_2$, $B_1 = B_2$ and pure FM is then $\theta_1 = -\theta_2 + \pi$, $B_1 = B_2$. Note that the addition of the unmodulated carrier does not affect the reconstruction of Eq.(3). This approach has been implemented using developed and thoroughly tested In-Phase/Quadrature Homodyne Separation (IQHS) algorithm illustrated in Figure 8. The first step of this algorithm is to eliminate the carrier frequency containing unwanted unmodulated signal by using homodyne shifting of the spectrum to zero frequency with respect to the carrier frequency. By doing so and filtering out unwanted higher frequencies and DC components after the homodyne procedure, both side-band components are shifted to the same modulating frequency: $(\omega \pm \Omega) - \omega = \pm \Omega$ and added together:

$$B_1 \cos(\Omega t + \theta_1) \pm B_1 \cos(-\Omega t + \theta_1) \quad (4)$$

Here "+" or "-" signs are determined by in-phase (cos ωt) or quadrature (sin ωt) multiplication, respectively, in the homodyning procedure. Squaring and extracting DC components from ± signals per the expression (2) yields respective AM and FM spectral component amplitudes defined by Eq.(1).

The MATLAB simulation of the IQHS for AM/FM modulated signals mixed with unmodulated carrier signal demonstrated its superior performance as compared with HT decomposition.
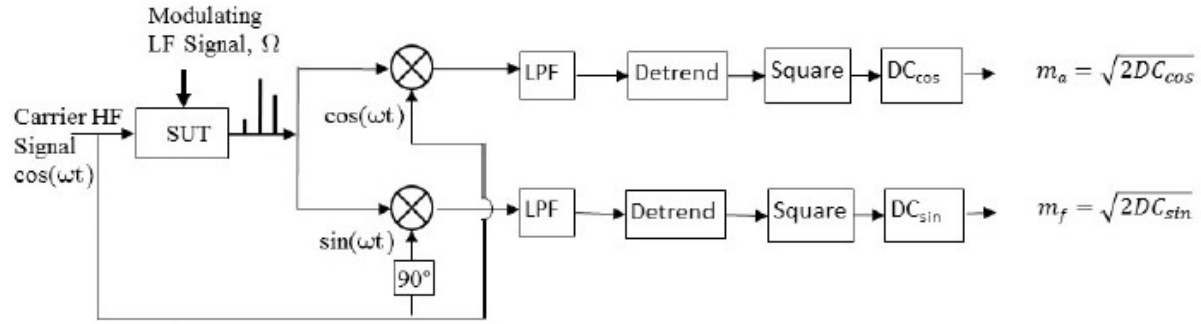
Figure 8. Diagram of In-Phase/Quadrature Homodyne Separation (IQHS) algorithm

Sweeping-Phase Homodyne Separation (SPHS) Algorithm

The IQHS algorithm works based on known modulation phase, φ_m. HT cannot detect this phase as it cannot distinguish between modulated and non-modulated carrier while IQHS algorithm is capable of recognizing the modulated carrier in presence of non-modulated carrier. The IQHS result is valid whenever the phase changes are negligible. It could be assumed that phase change is a very small number because of a small size of the tested samples and high speed of sound in steel. The IQHS algorithm as explained before works based on the multiplication of acquired modulated signal and background carrier signal in time domain. In order to practically use of this method in larger samples, the Sweeping-Phase Homodyne Separation (SPHS) algorithm has been developed.

Finding phase of a modulated carrier, modulation phase (φ_m), contaminated with a non-modulated carrier is problematic. Therefore, a sweeping-phase approach was developed to finding the DC components representing AM and FM components instead of applying IQHS. In the sweeping-phase homodyne separation (SPHS) algorithm, the reference signal is assumed to be a sweeping-phase signal which sweeps over sampling points of reference signal and generates a phase shifted reference signal. The result of DC component is expressed in relation to the sweeping modulation phase. The SPHS algorithm as shown in Figure 4.12 concludes multiple implementations of IQHS with phase shift of carrier signal to the next sampling point which results in sweeping phase of carrier signal. The precision of this approach is improved by increasing sampling points. While the sampling rate of used data acquisition board is 2 MS/s, the sampling point increased 5 times to 10 MS/s in which data points between original sampling points are added by means of interpolation. Using this modification, SPHS could be used to separate modulated signal to its valid AM and FM components. In addition, one important feature of the SPHS algorithm is that it can detect the phase of modulated carrier, which is involved in the modulation process, called modulation phase φ_m. The flowchart of SPHS algorithm is shown in Figure 9.

15

```
                          ┌─────────────────┐
                          │   Start SPHS    │
                          └─────────────────┘

      ╱───────────────╲              ╱───────────────╲
     ╱   Background     ╲           ╱    Acquired      ╲
    ╱   Carrier Signal   ╲         ╱    Modulated       ╲
    ╲                    ╱         ╲     Signal         ╱
     ╲──────────────────╱           ╲─────────────────╱

      ┌───────────────┐              ┌───────────────┐
      │   Increase    │              │   Increase    │
      │ Sampling Rate │              │ Sampling Rate │
      │by Interpolation│             │by Interpolation│
      └───────────────┘              └───────────────┘

                          ┌─────────────────┐
                          │      IQHS       │
                          └─────────────────┘

   ┌──────────────────┐
   │ Shift Carrier Signal │
   │  one sample point │   ┌─────────────────┐
   └──────────────────┘   │   Record MI,    │
                          │   AM and FM     │
                          └─────────────────┘

                              ╱─────────╲
              No             ╱ Phase Shift of ╲
         ◄────────────────── ╲  Carrier > 2π  ╱
                              ╲─────────╱

                               Yes

                          ┌─────────────────┐
                          │ Modulation Phase│
                          │   Measurement   │
                          └─────────────────┘

                          ┌─────────────────┐
                          │  Graphs of MI,  │
                          │   AM, FM,       │
                          │ and Modulation Phase│
                          │vs Cycle/Fatigue Life Time│
                          └─────────────────┘

                          ┌─────────────────┐
                          │    End SPHS     │
                          └─────────────────┘
```
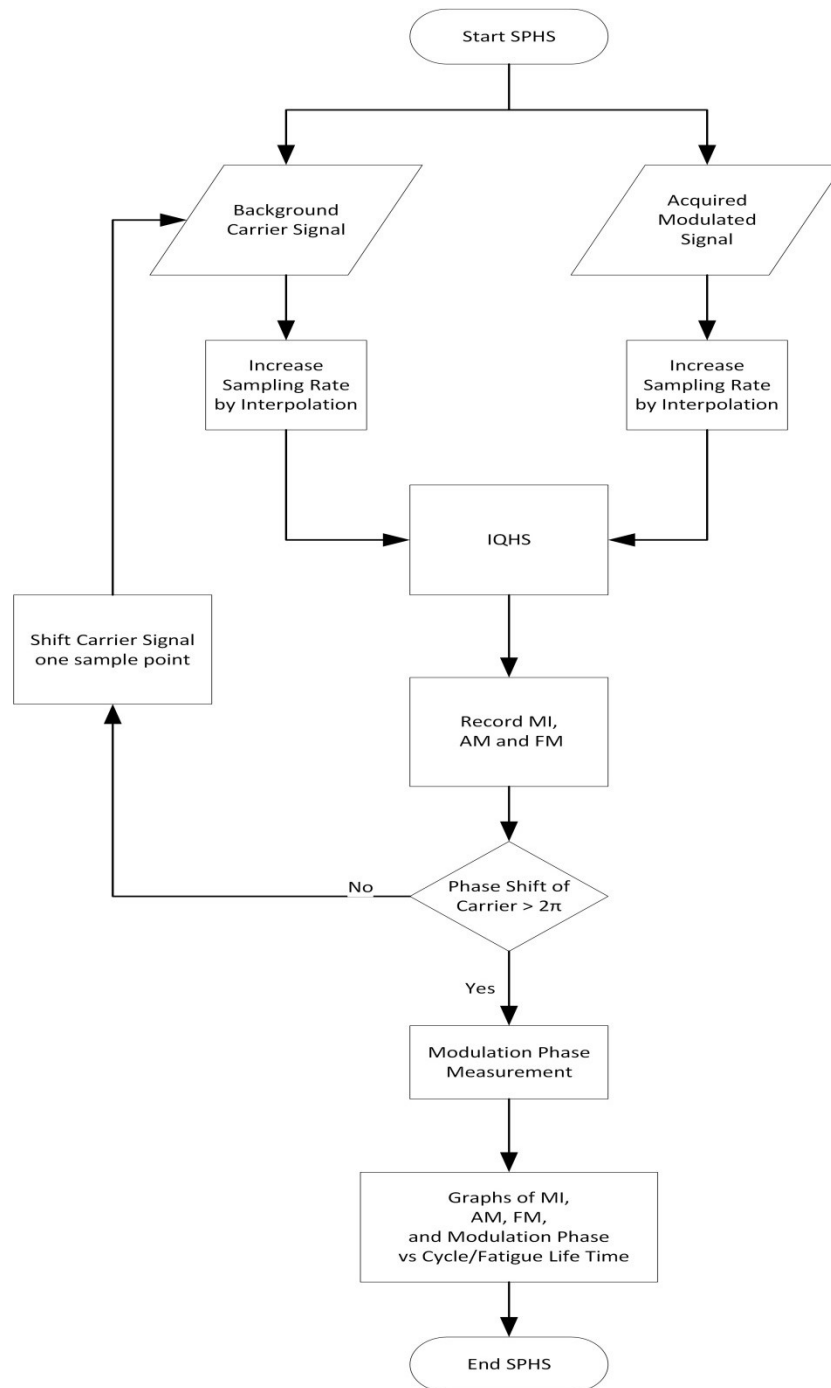
Figure 9. Flowchart of Sweeping-Phase Homodyne Separation (SPHS) algorithm.

In this process, the modulated signal received from system under test is multiplied by the background carrier signal, reference signal. Prior to this multiplication the sampling rate of acquired signals are increased in order to improve the precision of computations. After applying IQHS algorithm on these signals, MI, AM and FM components are recorded. Then the recurring algorithm continues the same process by shifting the reference signal to the next sampling point. After completion of this

16

recurring algorithm, the graph of MIs is depicted and the modulation phase (φ_m) and the valid AM and FM components corresponding to this phase are measured.

Enhancing the precision of the IQHS and the SPHS algorithms includes 1) resampling of the received signals, 2) using a low-pass filter, 3) optimizing the sample time, and 4) averaging the modulation indices.

Experimental Tests to Validate Algorithms
Fatigue failure is one of the most common failure modes of structural components; therefore, integrity of the structure depends on the prediction of fatigue cracks in early stages. The Vibro-Acoustic Modulation (VAM) method detects material defects by monitoring the modulation components generated by the interaction between a carrier (high-frequency ultrasound, ω) signal and a modulating (low frequency structural vibration, Ω) signal in the presence of various flaws such as fatigue and stress-corrosion cracks, bolted connections and delamination. The VAM method has been studied excessively to detect defects in a variety of materials.[49-54] Fatigue crack evolution in A-108 and A-36 steels is investigated using VAM method and an in-plane non-resonance very low frequency (10 Hz). Large numbers of samples have been tested to examine a) multi-path propagation of carrier signal, b) Modulation Index (MI) monitoring by VAM method, c) efficiency of the IQHS and SPHS algorithms in detecting cracks, and d) VAM sensitivity compared to Ultrasonic Testing (UT) and Eddy-Current Testing (ET) during fatigue cycling loading.

Two tests had been conducted to examine multi-path propagation of carrier signal in VAM output. As it was shown by modeling different scenarios in section 4.5, when the acquired signal consists a non-modulated carrier component, Hilbert Transform is unable to separate modulated signal to its valid AM and FM components. This limitation of HT in interpretation of VAM results necessitates development of new AM/FM separation methods. In order to explore the multipath propagation of carrier signal, two samples using 1- and 1/2-inch washers are used. The difference between these two samples arises from presence and absence of the non-modulated carrier in the output of system. The use of a 1-inch washer which covers all the samples path width is expected to result in complete involvement of carrier in the modulation process due to the contact between washer and the bar; thus, there would be no non-modulated carrier. On the other hand, using a 1/2-inch washer gives space to carrier to travel from contact-free parts of the sample; thus, it is likely to receive non-modulated carrier in the output.

A series of tests are explained below to implement VAM method on monitoring of crack evolution during fatigue cycling loading. In fatigue experiments, the modulation index, MI, is monitored for prediction of fatigue life time. Abrupt increase in the MI values considered as a sign of damage in the sample. In addition, IQHS and SPHS are used to separate AM and FM components.

17

MI Evolution During Fatigue Test

The initial objective of these tests was to do a life cycle analysis and assess the material degradation using the acoustical parameters obtained from the F-SCAN Vibro-Modulation system. For this purpose, improving the previous system in such a way that can calculate Modulation Index while utilizing fatigue cycling, 10Hz, instead of shaker, 300 Hz, was a milestone that had been reached. Moreover, recorded signals were needed for enhancing post processing method to separate AM and FM. To apply VMT method with IQHS and SPHS algorithms to the fatigue test specimens, several specimens have been tested.

Nonlinear Acoustic Vibro-Modulation System Setup

The test setup shown in Figure 10 consists of tension/compression testing system (MTS 810 servo-hydraulic Machine) capable of high cycle, low cycle fatigue and monotonic load testing, and the Nonlinear Vibro-Modulation system. The specimen to be tested is installed in the fatigue-testing frame, as shown in Figure 5.1(b).
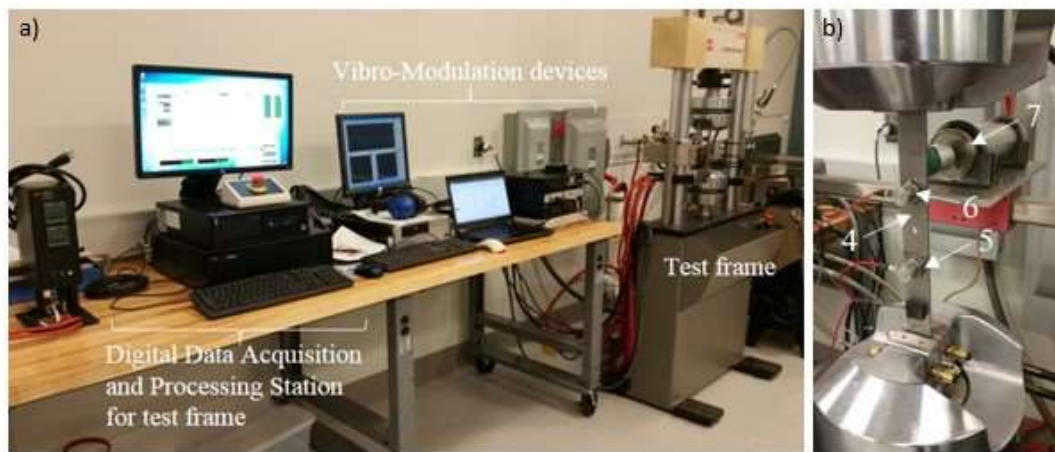

Figure 10. (a) Test setup and (b) a specimen mounted in fatigue testing machine

The calibrating specimen is a center notch specimen, as shown in Figure 5.2(b), which is equipped by IST universal sensor/transducers (annotated by 5,6).
The modulating signal is generated by a magnetostrictive shaker (annotated by 7) vibrations. The shaker is replaced by a low frequency vibration of cycling loading, 10 Hz, in order to enhance the VAM method to use structural vibration as modulating frequency. The small modulating signal also helps to eliminate the amplitude/phase frequency response effect on the output modulated result. All the test results presented here are conducted by using fatigue cycling as a source of the low frequency vibration to interact with the high frequency ultrasonic waves sent to the specimen. The vibration in this research caused by cycling loading is different than vibration caused by the shaker (Resonance Frequency), in this set of tests the test setup is closer to the actual field condition. The manufacturing of the specimen had been done in our laboratory.

The calibrating specimen is a center notch specimen, or an edge-notch specimen. Dimensions are given in Figure 11. The specimen is manufactured out of low-Carbon steel (yield stress 44 ksi). The advantage of the center notch or edge-notch specimen

is that first damage accumulation is expected to occur at the notch tip at half height of the specimen.
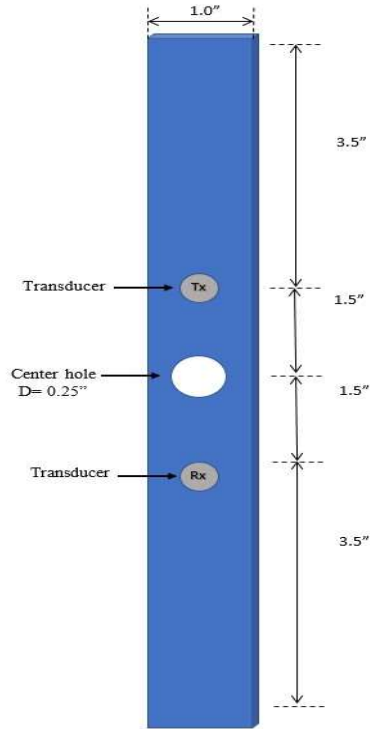
Figure 11. Sample geometry of test coupon

The applied VAM technique in this study consists of a computer with a LabVIEW F-scan software that generates the carrier signal. This occurs via Data Acquisition board (DAQ) and the high frequency amplifier that are connected to the computer as shown in the Figure 12(d). The amplified high frequency signal is introduced to the sample by the transmitter transducer (Tx). The received modulated signal will be transmitted to the DAQ via the receiver sensor (Rx). The typical specimens under tests are 1" by 10" rectangular bars of 1/8" thickness and 1/4" diameter center-notch.

The VAM for Fatigue Damage Evolution
Fatigue tests were conducted using an 810 MTS test frame connected to a digital data acquisition and processing station. The specimens were mounted parallel to the applied load. A 10 Hz tension only low-load fatigue cycling was used for the measurement purposes. The applied tensile loads during the initial tests are a maximum of 20 kN and a minimum of 0 kN.

Figure 12. VAM equipment setup for fatigue tests: (a) data acquisition board (DAQ), (b) high frequency amplifier (HFA), (c) specimen installed in MTS 810 machine for tension only fatigue test and (d) simple connection diagram
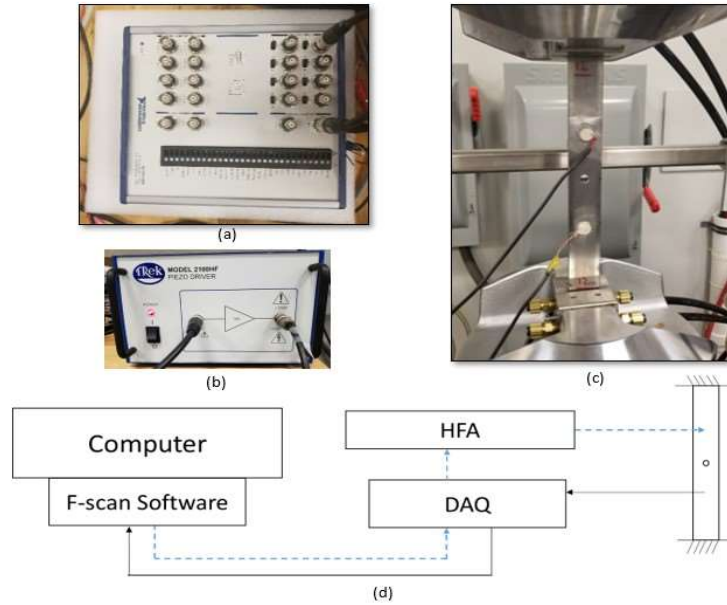
Since in fatigue tests, results of different but identical tests might differ widely, statistical interpretation by the designer is needed.[55] From the initial estimations maximum tension load was set to 20 KN and minimum load was set to 0 KN for all of the specimens. The fatigue test was designed to be conducted as a tensile only(R=0). Thus, R (ratio of minimum stress to maximum stress) is equal to zero As shown in Figure 13. Recommended cycling loading frequency of fatigue experiment is 0.01 to 100 Hz due to limitations of servo-hydraulic testing machines.[56] Also, higher cycling frequencies would affect the experimental results because of temperature effect in the vibrational loading regime. Our chosen frequency for fatigue experiment, 10 HZ, is in the recommended range. After several trials for the same specimen, with the same fatigue parameters, the range of the number of cycles to the failure was estimated between 30000 to 40000 cycles.
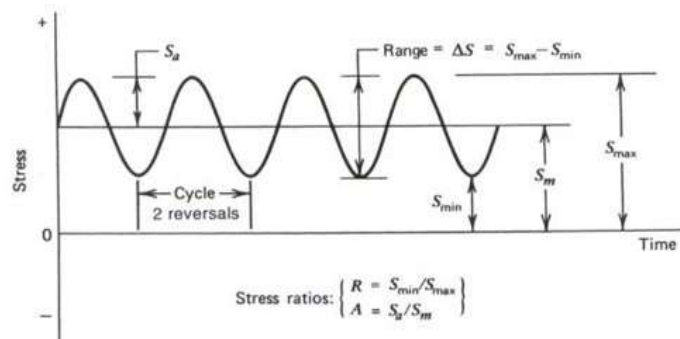

Figure 13. Cycling loading parameters in fatigue experiments

Before starting the fatigue test, the amplitude-frequency response of mounted sample is measured for applicable frequency range of sensors, 120 to 200 KHz. One example of the recorded frequency response is shown in Figure 14. Since the representative MI value is obtained by averaging of MI values on a 5 KHz frequency range, the signals should be selected in the flat area of frequency response of sample to avoid effect of amplitude and phase frequency response on sideband amplitudes. Moreover, 10 Hz modulating frequency decreases the effect of frequency response on sidebands due to small differences between sidebands and carrier amplitudes. In this case, the range of 165 kHz to 170 kHz is selected to measure MI values. Chosen frequency needs to be smooth and close to zero dB.
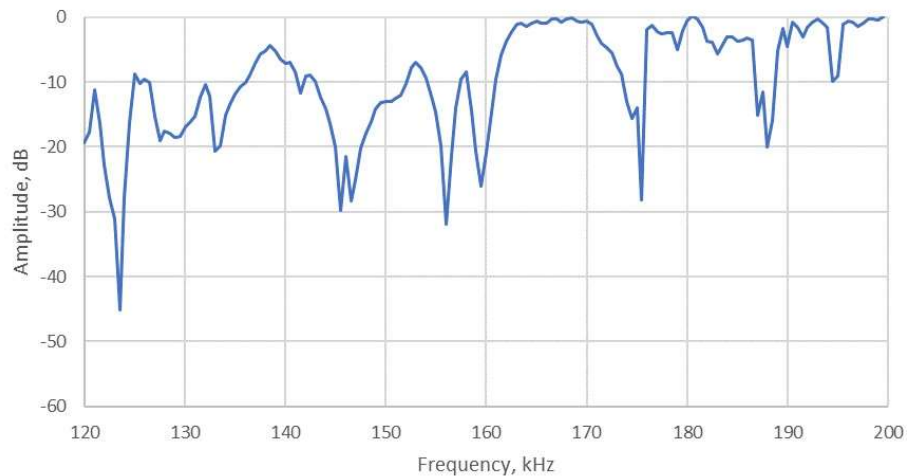

Figure 14. Frequency response of a sample for frequencies between 120 KHz and 200 KHz with 500 Hz steps

For recording the modulation index values, a maximum tension load of 1 KN and minimum load of 0 KN is applied with the same frequency of 10 Hz during the measurements. The initial measurements will be conducted with the mentioned setup, before staring the main test that would be called cycle zero. For post-processing purposes 5 signals at specific frequencies have to be recorded for each test. For choosing proper frequencies for recording signals, some characteristics need to be considered such as having the sidebands in a flat range to eliminate the effect of frequency response on the measured sidebands since I realized that frequency response will affect the measurements. In future, the effect of frequency response on the sidebands has to be considered.

The results obtained from six of the conducted tests are visualized as a modulation index vs number of fatigue cycle/fatigue life time graph in Figure 15. Six of the fatigue test monitoring by VAM method are represented here. For all of them, I applied the same high load of 20 KN as maximum tension and 0 KN as minimum load for the fatigue. The results from the tests confirm one of our initial assumptions that utilizing fatigue cycling would work well with the current system; since MI changes are consistent with the material degradation process. In order to be able to compare the

21

data from all of the tests, the data are normalized to the number of fatigue cycles and Initial Modulation Index of -60 dB.

The resulting filtered and normalized graph of the modulation index vs number of fatigue cycles reveals a relatively consistent set of trends for different conducted tests. These results show that besides the gradual increase in MI during the fatigue test, for most of the specimens after 80 percent of their life, a significant increase is observed in the MI values. This abrupt MI change is a sign of damage in the sample; therefore, the failure of the sample could be predicted 20% in advance of failure.
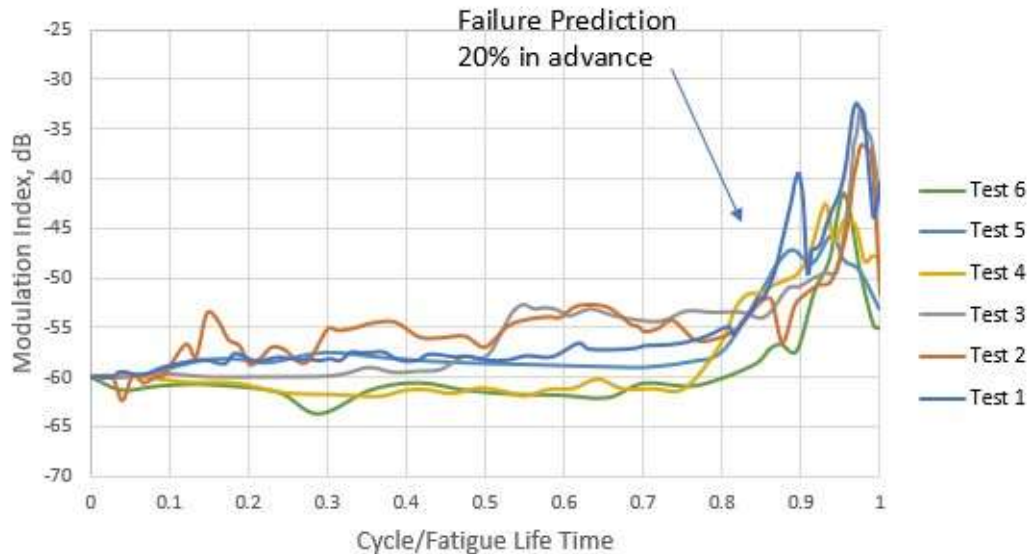
Figure 15. Modulation Index, Normalized to initial MI = -60 dB vs Number of fatigue cycles

For the first cycles, as it is observed in most of our findings, some significant changes might occur on the initial modulation index values due to high level and unpredictable variations of background modulation. The contact nonlinearity between the clamps of fatigue machine and the specimen could be one of the reasons. However, this will be fixed after a couple of cycles. Then the trend would look like the normal trend.

Sample Thickness Effect on VAM
The thickness of sample is varied to explore the thickness effect on the VAM output. The sample geometry is identical to the typical center-hole specimen; however, the sample thickness is doubled and is 1/4 inch. Because of the doubled section area, the applied fatigue load is also doubled (40 KN) in order to maintain the same maximum tensile load. Figure 16 shows this sample during the fatigue test.
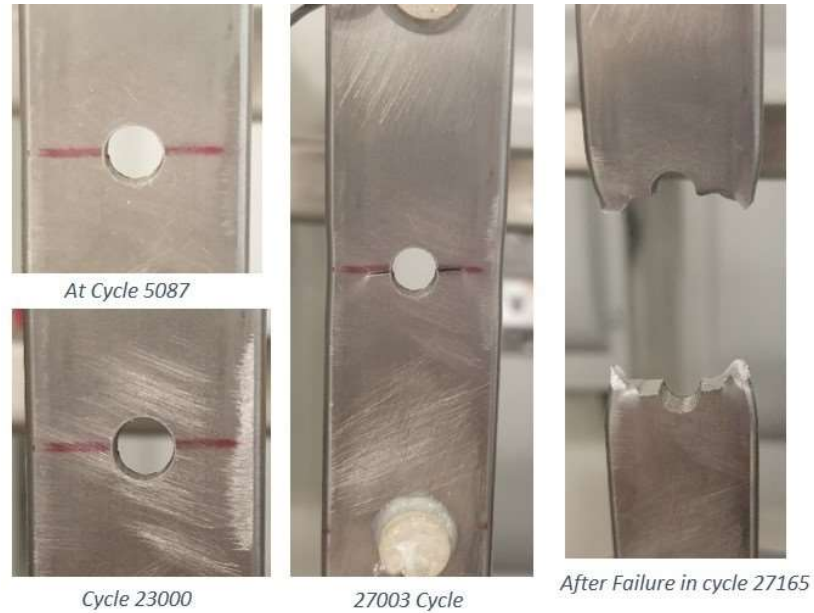
Figure 16. Sample with 1/4-in thickness at different fatigue cycles

The resulting modulation index evolution throughout the fatigue life is shown in Figure 17. Noting the steep increase of MI as soon as 80% of life time has passed, we can conclude that the sample thickness does not influence the VAM results regarding monitoring of damage evolution during fatigue loading.
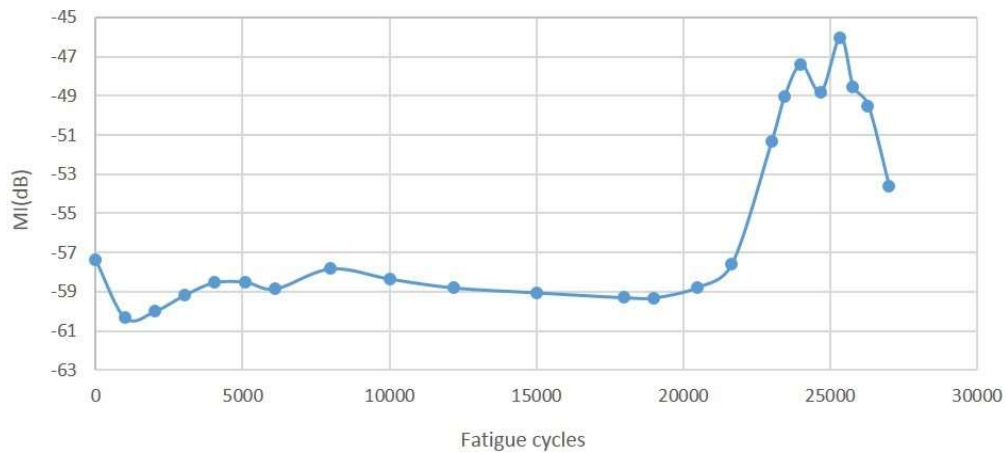
Figure 17. Modulation Index vs Number of Fatigue cycles for Sample with 1/4 in thickness

Multi-path Propagation of Carrier Signal
As explained in subsection 4.1.2, the non-modulated carrier that is not involved in the modulation process appears as an extra carrier signal in the received modulated signal. The superposition of this non-modulated carrier with modulated carrier which is involved in the modulation process results in erroneous results of AM/FM separation

using HT demodulating method. This non-modulated carrier travels to receiving transducer through intact areas of the sample. This multi-path propagation effect is difficult to investigate during fatigue tests; therefore, a test is designed to explore the multi-path propagation effect. A sample with 10 in length, 1 in width and 1/8 in thickness is prepared from steel A-108 and a hole is placed in the middle of sample. The sample is vibrated with a low fatigue loading with 10Hz cycling frequency; this low vibration parallel to the sample direction generates the modulating signal as it is present in fatigue experiments. This sample is tested separately when a bolt connection is installed on the middle hole with a 1-in washer and a 1/2-in washer shown in Figures 5.9(a) and 5.9(b), respectively.

Bolt Connection with 1-inch Washer

The sample is covered in the bolt connection area by a 1-in washer; so, the whole path of signal from transmitter to receiver is covered by the washer which results in the modulated output. The carrier signal will be modulated by modulating signal in presence of contact-type nonlinearity such as bolt connection. Using a large 1-inch washer covering the whole sample width results in passing the whole signal through the connection. The whole covered path prevents presence of nonmodulated carrier in the receiver. The acquired signal is a prevailing AM modulated signal without additional non-modulated carrier. The sample is shown in Figure 18 (a).
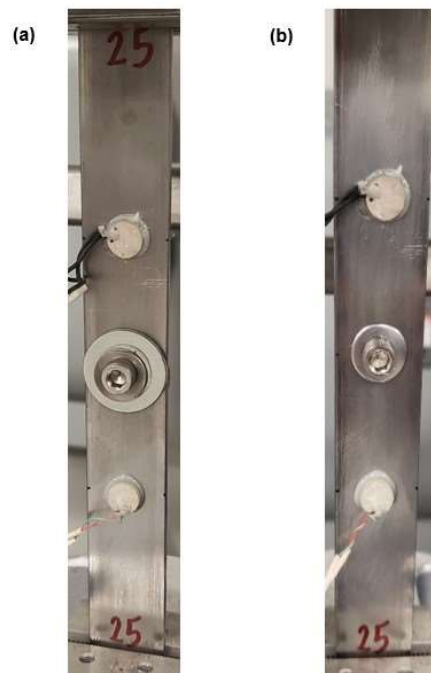

Figure 18. Bolt connection with (a) 1-inch and (b) 1/2-inch washer

The acquired signal in time domain is illustrated in Figure 19. The signal shows prevailing amplitude modulation, AM. The varying amplitude of signal is a sign of high AM component in the output signal; this amplitude variation can be expressed by envelope function.

24
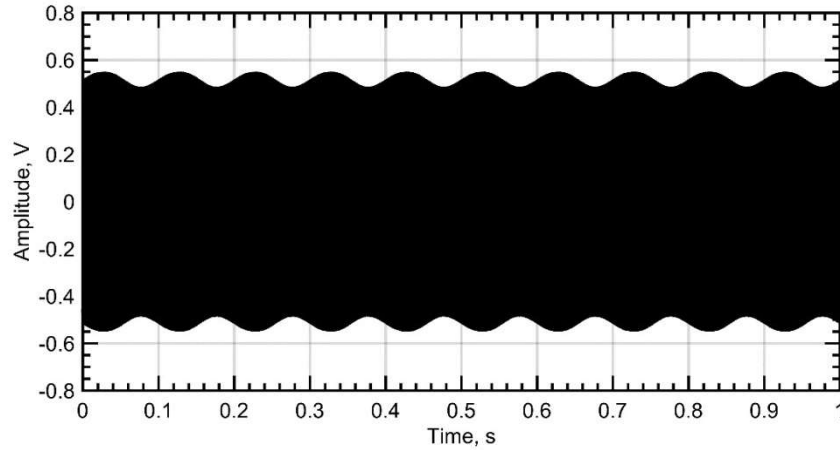
Figure 19. Received signal from sample with bolt connection

The received signal is then processed to measure MI using four different approaches: a) Fourier Transform (FT), b) Hilbert Transform (HT), c) envelope function, and d) Sweeping-Phase Homodyne Separation (SPHS). Subsequently, AM and FM separated components are measured by SPHS and HT demodulating. These results are shown in Figure 20.

Firstly, the modulation index, MI, is measured by Fourier Transform (FT) spectrum. Modulation Index is evaluated directly by the relative amplitude of sidebands components to the carrier component:

$$MI = 20 \log_{10}(\frac{B_1 + B_2}{2A}) \tag{5}$$

B_1 and B_2 are the amplitude of higher and lower sidebands and A is the amplitude of carrier frequency.

Secondly, MI is measured from envelope function. Usage of a 1-inch diameter washer results in modulation of the whole signal passing through the connection and absence of non-modulated carrier. Modulation Index could be measured by subtracting the maximum and minimum of envelope function.

$$MI_{envelope} = \frac{1}{2}\frac{max(env) - min(env)}{max(env) + min(env)} \tag{6}$$

Figure 20 enlarges the envelope function of the received signal. The maximum and minimum of envelope is measured as 0.545 and 0.481, respectively. The MI value measured based on Equation (5.3) would be 0.031.

25
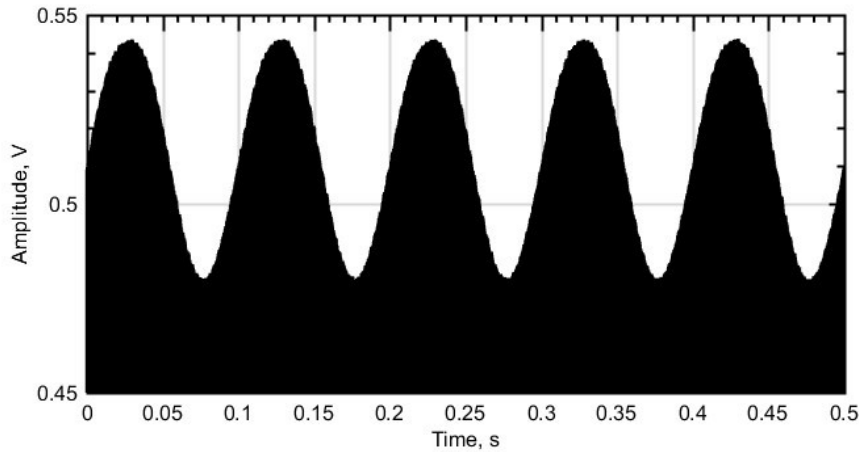
Figure 20. Magnified waveform of sample with bolt connection

After measuring MI values with FT and envelope function analysis, SPHS and HT are used to decompose the modulated signal to its AM and FM components. The MI could also be measured based on this AM/FM separated values to be compared with FT and envelope function results. SPHS can be used to compensate for distortions due to a non-modulated carrier with unknown initial phase. In this approach, the signal is multiplied by a sweeping-phase reference signal instead of multiplying signal with in-phase and quadrature reference signal. When the sweeping-phase reference is completely in-phase with the received signal, sweeping modulation index (M_i) represents AM component of the signal and when the sweeping-phase reference signal is in quadrature phase difference with the received signal, sweeping modulation index (M_i) represents FM component of the signal. The AM and FM components appear as the maximum and minimum of the DC component of sweeping algorithm as shown in Figure 21.

Figure 21. SPHS result of bolt connection with 1-inch washer with respect to sweeping-phase reference signal

26

Figure 21 shows M_i results of SPHS in a bolt connection with 1-inch washer with respect to initial phase of the reference carrier, modulation phase.
The extreme values of sweeping modulation index are corresponding to the AM and FM components. When the results of the M_i start from o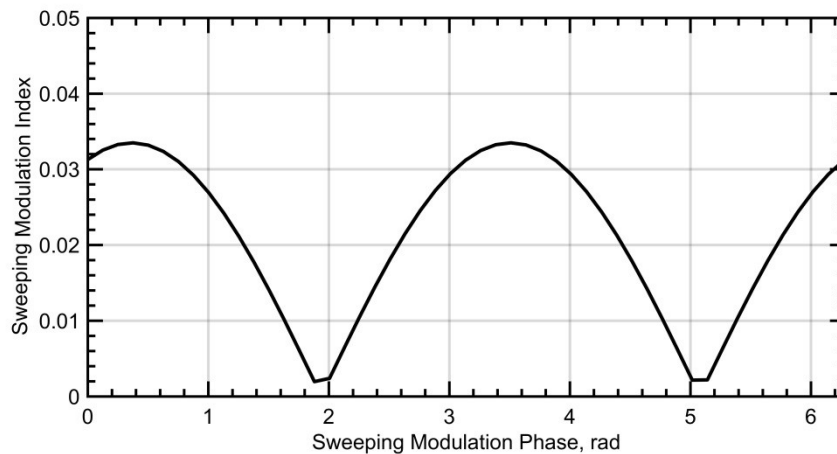ne of these extreme values, it shows that there is no non-modulated carrier to change the phase of the superposed carrier. Therefore, the phases of the reference carrier and the modulated signal are the same as the modulation phase. The SPHS results show that the sweeping modulation index, M_i, starts from maximum which is an indication of absence of phase shift and non-modulated carrier.

The HT demodulating results of the received signal is measured and MI values are measured from AM and FM components. The MI results of four processing approaches: a) FT, b) envelope function, c) SPHS, and d) HT are shown Figure 22. The four measurements of MI are very close to each other, as expected. Using a large washer will result in modulation of almost the whole signal, which passes through the bolt connection (there is no path for signal to avoid modulating). Accordingly, the non-modulated carrier has exceedingly small amplitude. Therefore, the separated AM and FM components show almost identical results. Only the modulated carrier was expected when using a 1-inch washer, and this was confirmed when identical MI measurements were obtained by different approaches.
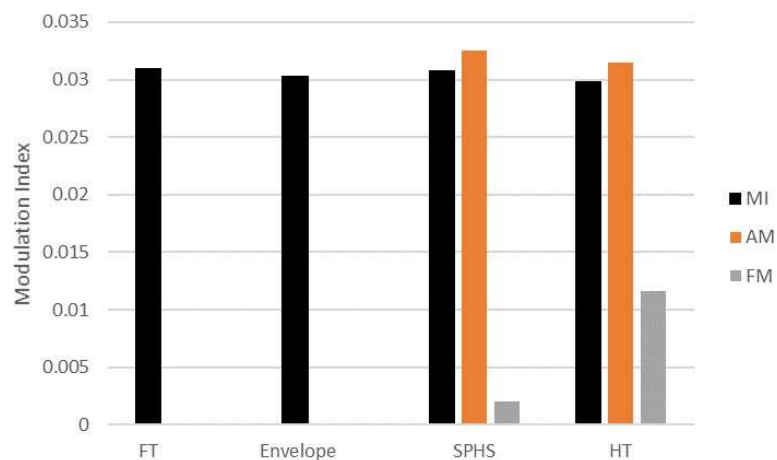
Figure 22. MI measured by (a) Fourier Transform, (b) direct envelope measurement, (c) SPHS and (d) Hilbert Transform for a sample with 1-inch washer

Bolt Connection with 1/2-inch Washer
The same sample with bolt connection and 1/2-inch washer, as shown in Figure 18(b) is tested. The cycling load with 10 Hz frequency generates the modulating signal. Since the whole path of signal from transmitter to receiver is not covered by the 1/2-washer which produces contact-type nonlinearity, the presence of non-modulated carrier in the received carrier is expected. The presence of non-modulated carrier

influences the amplitude and phase of superposed modulated carrier. The HT should not be capable of demodulating the acquired modulated signal due to this non-modulated carrier.

It should be mentioned that FT and envelope analysis will not reflect the correct MI values in presence of non-modulated carrier; if it is assumed that the carrier involved in modulation is contaminated by an additional non-modulated carrier as shown in Equation (4.22).

The presence of non-modulated carrier is distorting the amplitude and phase of carrier signal; therefore, MI calculated via "Fourier transform" is not reflecting valid modulation index. In contrary, decomposition of the modulated signal to its AM and FM components by SPHS algorithm explains the correct modulation nature of the signal.

Figure 23 shows M_i result of bolt connection with 1/2-inch washer. The SPHS results show that the sweeping modulation index with reference to sweeping modulation phase does not start from maximum which is an indication of the presence of phase shift and therefore non-modulated carrier. In fact, the phase of superposed carrier is different than the modulation phase because of non-modulated carrier.
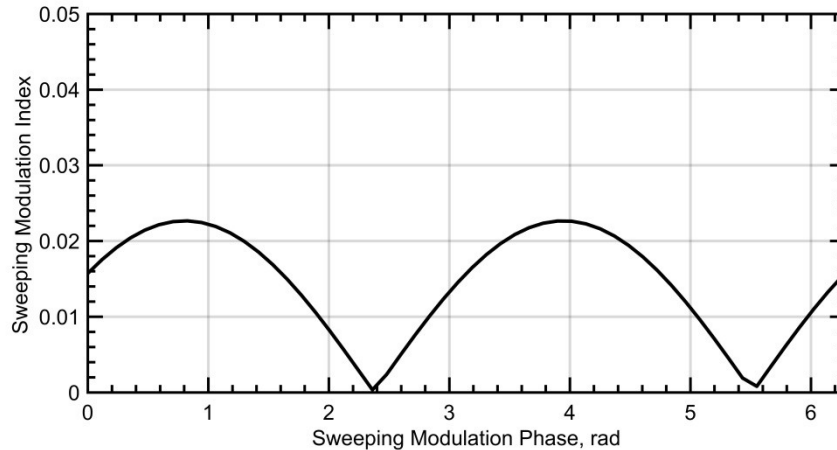
Figure 23. MI result of bolt connection with 1-inch washer with respect to sweeping-phase reference signal

In using a 1-inch washer, we expect to receive only modulated signal since our samples width is 1 inch and there is no path for the signal to avoid modulating. In this case, our approach and Hilbert Transform should show almost identical results. On the other hand, the 1/2-inch-diameter washer not covering the whole sample width should cause a non-modulated carrier. Hence, I expect discrepancies in SPHS and HT results, as shown in Figure 24. It is expected that AM component dominates the received signal because of the contact-type nonlinearities; therefore, Hilbert Transform reveals improper decomposition result. Note that HT is not capable of demodulating the received signal to its components.

AM and FM Separation during Fatigue Damage Evolution

After successful implementation of VAM method in detecting flaws during fatigue experiment of simple samples, efforts were focused on practical usage of this method on condition with high initial nonlinearity due to contact-type nonlinearity such as bolt connections. The IQHS and SPHS algorithm are developed in MAT-LAB as well as HT method for AM/FM separation.

The IQHS Implementation

A test was designed to observe AM and FM dynamics during tensile fatigue of a A-108 steel bar as shown in Figure 25. The thickness, width and height of the under-test sample are 1/8 in, 1 in and 10 in, respectively. No bolt is attached to the sample. The test is a tension-only fatigue test with fatigue loading of 0 to 20 KN and fatigue frequency of 10 Hz. The AM/FM separation has been processed by IQHS algorithm.
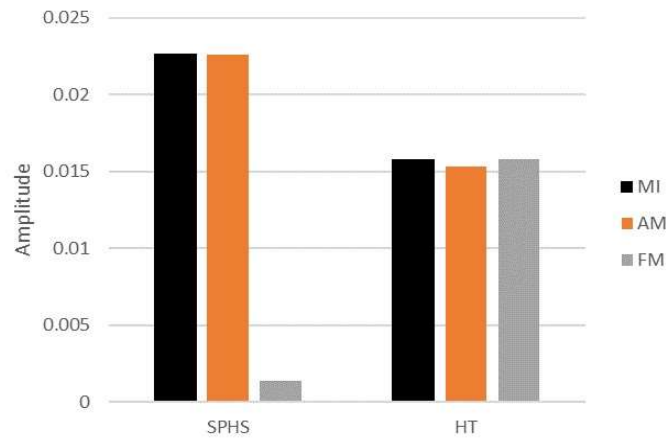

Figure 24. MI and AM/FM components measured by a) SPHS, b) Hilbert Transform.
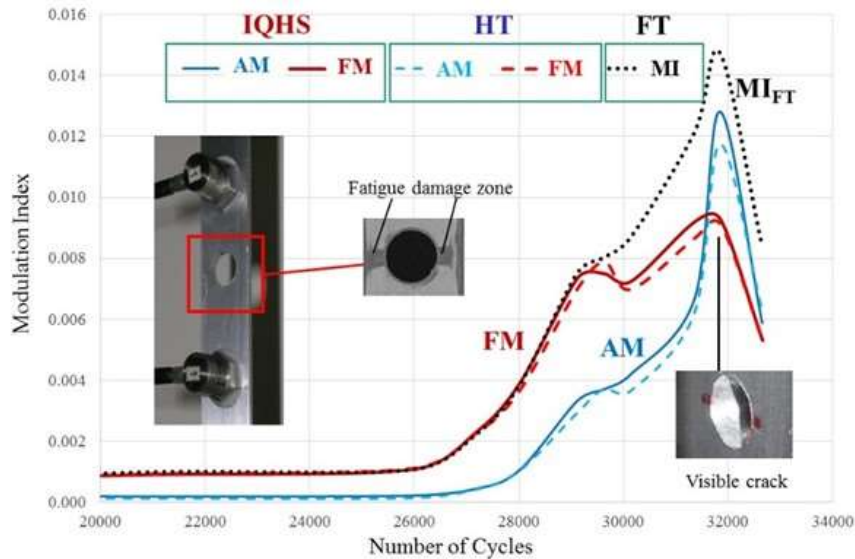

Figure 25. AM and FM growth during fatigue accumulation

29

The damage was accumulated across the bar near the central hole (damage zone is shown as a grey area obtained by the ultrasonic microscope) so that there were no non-modulated paths, and, therefore, IQHS and HT comparison can be made. The results validated our hypothesis that initial damage produces primarily FM modulation which is taken over by AM modulation as visible contact-type defect (crack) has developed. The results show that even though both AM and FM components have a very low value at the beginning of the test, the FM component starts increasing prior to formation of any visible macro cracks. After growth of the macro crack, the AM component dominates the FM component. It should be mentioned that AM and FM components are both normalized to the amplitude of the received signal.

Another test presented here demonstrates ability of the developed algorithm to detect early damage evolution (FM signal) in the presence of AM strong structural nonlinearity such as bolted connection, as shown in Figure 26. In this specimen, the bolt connection near the area of the central hole introduces initial high nonlinearity to the MI readout of the sample, such that MI increase could not be observed as the sign of damage accumulation. However, while the AM component of the modulated signal shows the contact-type nonlinearity as the initial high value, FM component is a very small value. The FM increase should be considered as the indicator of micro damage accumulation in the sample before the crack could be visible.
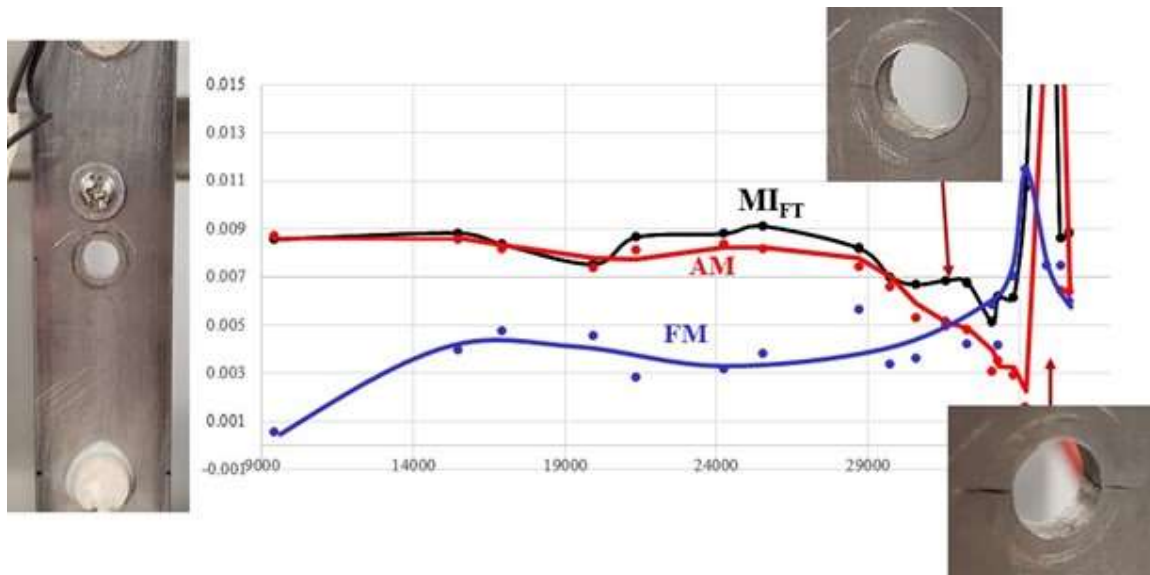
Figure 26. Damage detection (FM) in the presence of a strong AM signal from structural nonlinearity (bolted connection)

The SPHS Implementation

ASTM A-36 is the most commonly used mild and hot-rolled steel. It has excellent welding properties and is suitable for grinding, punching, tapping, drilling and machining processes. A-36 can be galvanized to provide increased corrosion resistance. A-36 bars with 1/8-in thickness and 1-in width are used for following

experiments instead of A-108 steel. The consistency of all results proved that steel type could not make any issue in regard to application of VAM technique.

The primary experiments show the ability of IQHS algorithm to demodulating AM and FM components of the acquired signals in the VAM method. The IQHS algorithm is working based on known modulation phase, φ_m. The IQHS result is valid whenever the phase changes are negligible. It could be assumed that phase change is a very small number because of small size of the tested samples and high speed of sound in steel. In order to enhance VAM method to a global detection method without knowledge of modulation phase, the Sweeping-Phase Homodyne Separation (SPHS) algorithm has been developed. SPHS is capable of separating modulated signal to its valid AM and FM components in presence of non-modulated carrier. Moreover, the SPHS can detect modulation phase, involved in the modulation process. In the following test series, AM and FM components separated by SPHS are inspected as well as modulation phase changes during damage accumulation.

Sample without connection

A sample is tested under 20 KN tension only cycling loading to validate the improvement of SPHS algorithm and to investigate modulation phase evolution during the fatigue experiment. This sample is made of A-36 steel. Length, width and thickness of sample are 10 in, 1 in, 1/8 in, respectively. A hole is made in the middle of sample to control the fracture area as depicted in Figure 27(a). The crack in the vicinity of central hole is also shown in Figure 27(b).
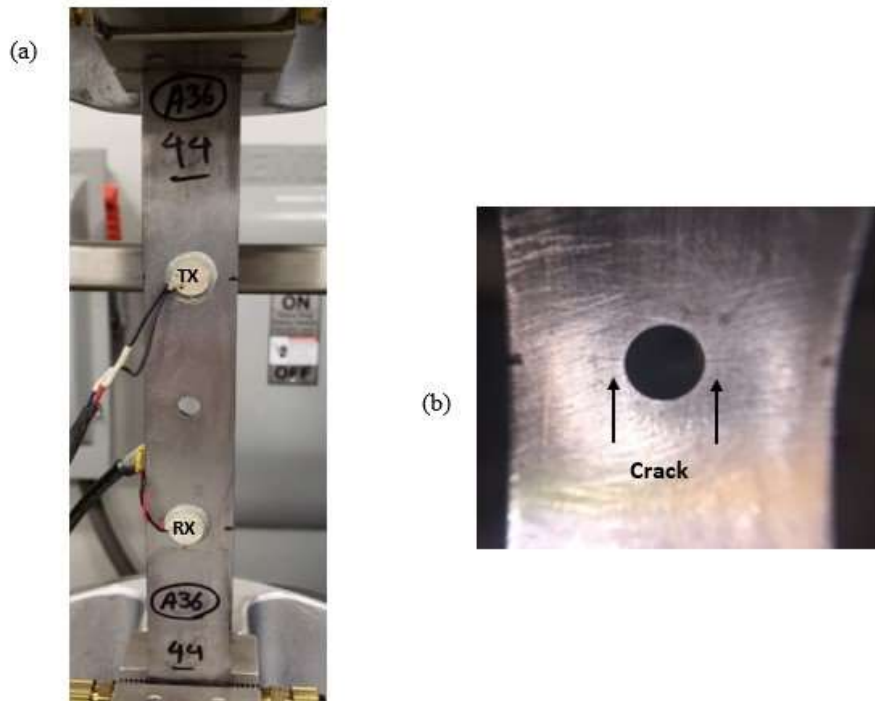

Figure 27. (a) Sample without connection under fatigue test with 20 KN tension only cycling loading and (b) visible crack at the 44057 cycle (95% of fatigue life time)

The processed results of SPHS method are shown in Figure 28. All results are shown with respect to cycle/Fatigue Life Time. The sample failed after 46339 cycles and the crack was visible at the 44057 cycle which is approximately 95% of fatigue life time. Figure 28 (a) shows the AM and FM components of the acquired signal processed by SPHS algorithm. While the AM component is dominant in the recorded signals of fatigue experiment as it is almost equal to the MI value due to small contribution of FM components, the FM is present and contributes to the modulated signal as well.
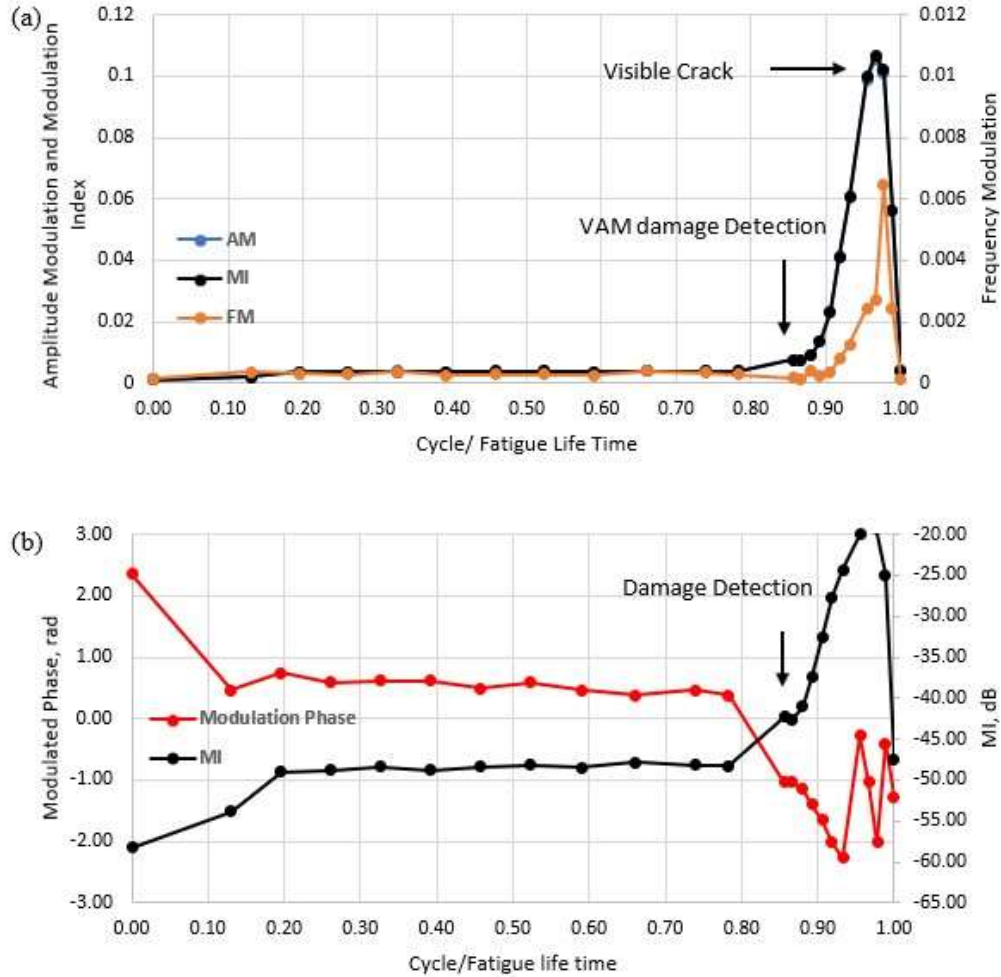
Figure 28. (a) AM/FM separation of the sample without connection and (b) modulation phase detection

A similar pattern, specifically an increase in the value after formation of micro-cracks, is observed in all three measurements of MI, AM and FM components. In addition, the modulation phase of the signal is measured during the fatigue cycle. Interestingly, the modulation phase is almost constant prior to formation of crack and increase in the MI value. After formation of the micro-cracks, the modulation phase starts to continuously decrease. The fluctuations in the modulation phase are observed after the crack is visible and opening and closing of the crack occurs.

Another sample without any connections with the same dimensions of the previous sample is tested to observe the SPHS results of low cycle fatigue as it is shown in Figure 29 (a). This sample was going through 26 KN tension only cycling load. This high load leads to low cycle failure of the sample at cycle 13802. When a component is subjected to low cycle fatigue, it is repeatedly plastically deformed. The crack was visible at cycle 12773 which is approximately 93% of fatigue life of the sample (Figure 29(b)).

The AM and FM components separated by SPHS and the MI increase of this case is not as clear as the previous results as shown in Figure 5.20(c) but consideration of modulation phase shows that the continuous change in the modulation phase to the lower values could be a very strong sign of damage presence in the structure. Figure 5.20(d) shows modulation phase changes after micro-crack formation.
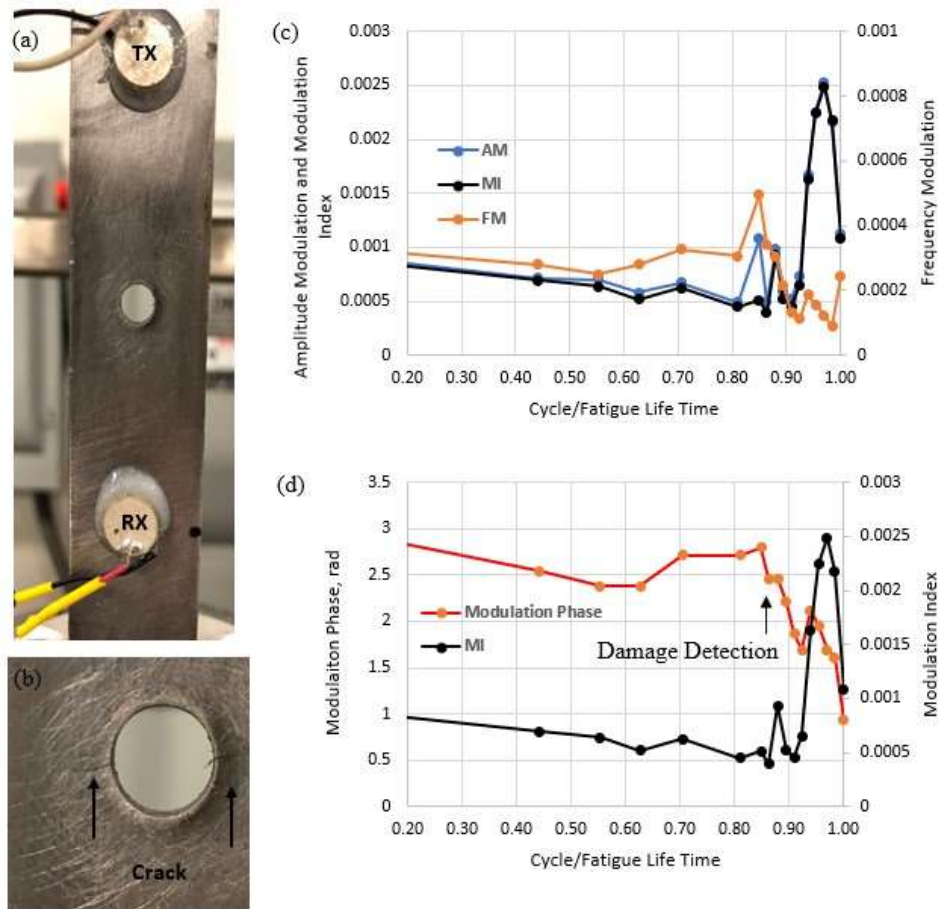

Figure 29. (a) Simple sample under fatigue test, 26 KN tension, cycling loading, (b) visible crack at the 12773 cycle (93% of fatigue life time), (c) AM/FM Separation of frequency 198.5 kHz and (d) Modulation phase detection of frequency 198.5 kHz

<u>Sample with connection</u>

Various samples with connections were tested to investigate the SPHS algorithm results. Length, width and thickness of samples are 10 in, 1 in, and 1/8 in. A hole is made in the middle of samples similar to the previous samples to control the fracture. A connection is designed as shown in Figure 30 with the same ASTM A-36 material and installed on the middle hole.
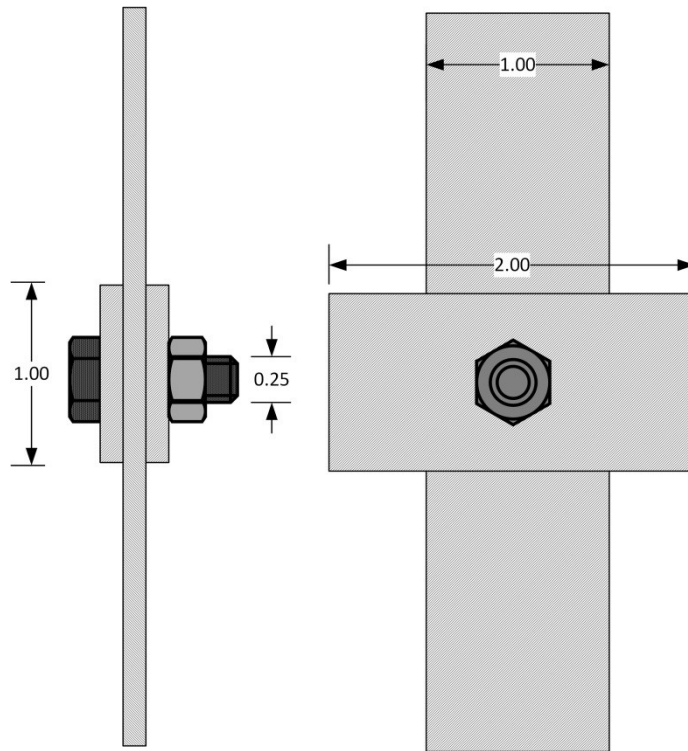
Figure 30. Schematic of the connection with generated contact perpendicular to the vibration direction

Two pieces of 2-inch long bar are used as a contact-type connection in both side of the bar which is under cycling loading. This connection is attached to the sample using bolt and nut. Thus, all the generated contacts between connection bars with the sample and with bolt and nut are perpendicular to the vibration direction. The attached connection shown in Figure 31(a) introduced a very high initial nonlinearity level of the MI measurements. The MI stays at -32 dB in this sample (Figure 31(b)) whereas the MI was -55 dB in the simple sample without connection (Figure 28(b)).

However, while the high nonlinearity level in presence of connection makes the MI readings unable to predict the failure of structure as depicted in the Figure 31(b), the modulation phase changes can elaborate the crack growth in the sample during fatigue cycles as shown in Figure 31(c).
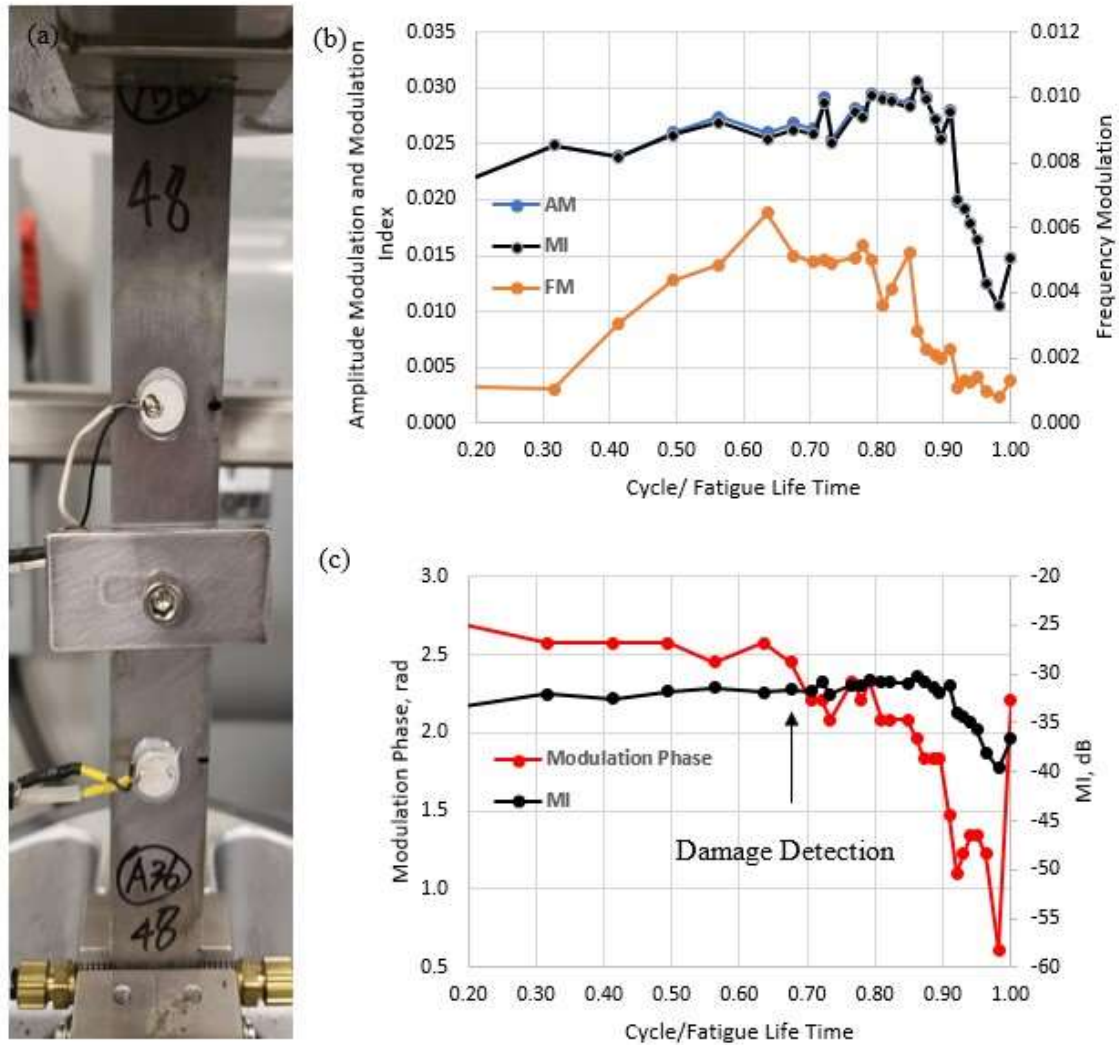
Figure 31 (a) Sample with designed connection (contact parallel to vibration) by initial high level of nonlinearity less than 20 KN tension-only cycling loading, (b) AM/FM Separation of 195 kHz frequency, and (c) Modulation phase detection of 195 kHz frequency

In another example a threaded-hole connection is considered. The hole is threaded by tap NF #28. First, the screw is attached to the sample without any usage of nuts at the end as shown in Figure 32(a).
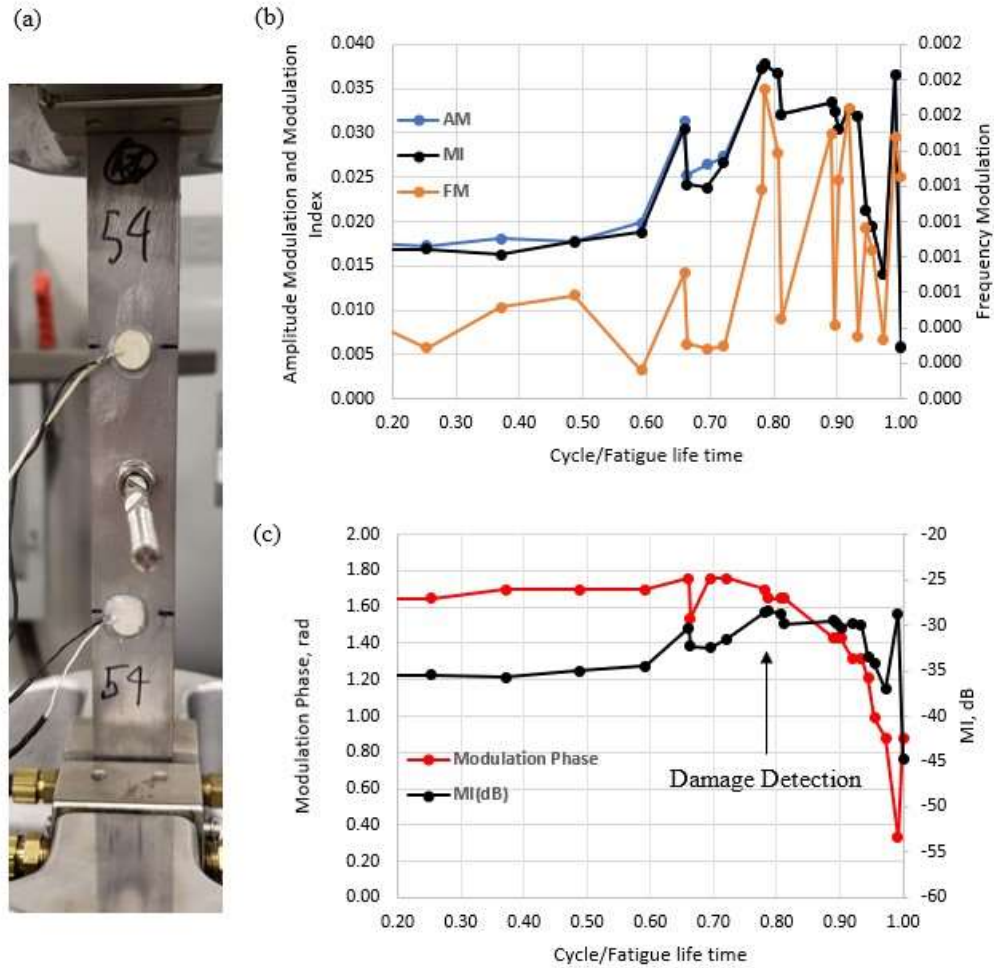
Figure 32 (a) Sample with screw only (contact perpendicular to vibration) direction showing an initial high level of nonlinearity under 20 KN tension only cycling loading, (b) AM/FM separation of 175 kHz frequency, and (c) modulation phase detection

In usage of screw without nut, the prevailing contact is in the threaded parts, perpendicular to the vibration direction. The MIs of VAM method show an initial high level of nonlinearity as shown in Figure 32(c). This high level of nonlinearity obscures VAM capability of detecting cracks by monitoring the MIs. The MI increase could not be observed due to presence of contact-type nonlinearities.

While interpretation of MI and AM/FM separation results is very challenging, the modulation phase could be a sign of crack formation in the sample as shown in Figure 32(c). By continuous monitoring of modulation phase, it is observed that modulation phase starts decreasing in the early stages of crack formation. The continuous decreasing of modulation phase after a few steps is indicative of damage.

In another sample as shown in Figure 33(a), the screw is supported with washer and nut. The difference between this sample and the sample showed in Figure 32(a) arises from contact direction. While contact was perpendicular to the vibration direction in the

36

previous sample, a mixture of contacts parallel and perpendicular to the vibration is present when a screw and nut is used. Again, the results show the high initial nonlinearity due to the contact-type connection as shown in Figure 33. Therefore, damage cannot be detected by monitoring the MI increase of VAM method. The FM component calculated using SPHS algorithm shows an initial increase in the 70% of fatigue life time which appears to be the damage indication. Despite the challenging interpretation of AM/FM separation results, the decreasing trend in modulation phase shown in Figure 33(b) measured using SPHS method reveals the damage accumulation in early stages of fatigue crack growth.

If FM component evolution could be assigned to the crack growth in the sample, the modulation phase changes would be a more reliable damage indicator of micro-defect formation. In all tested samples modulation phase starts decreasing prior to any visible crack or damage. It appears that the modulation phase changes correlates to micro-crack formation. As such, it is a robust method of detecting damage in the sample and it can provide earlier sign of crack than either MI or AM/FM observations.

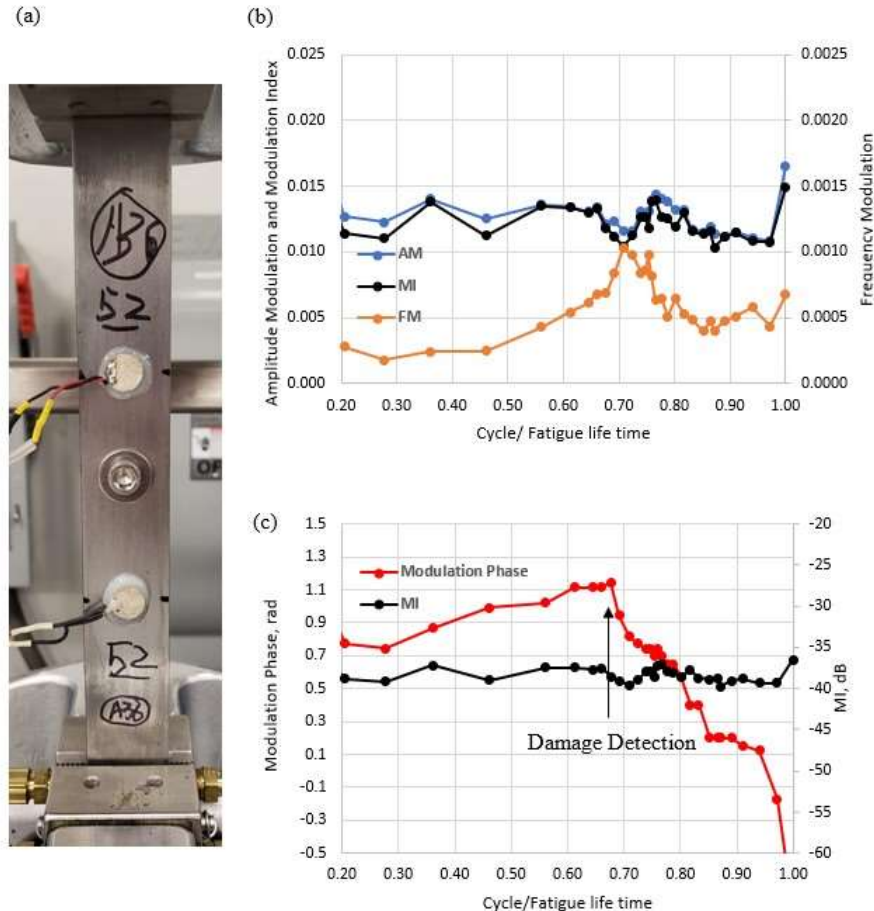Figure 33. (a) Sample with screw and nut connection (contact is both parallel and perpendicular to vibration) showing an initial high level of nonlinearity under 20 KN tension only cycling loading, (b) AM/FM separation of 188 kHz frequency, and (c) modulation phase detection of 188 kHz frequency

37

Study of Various Conditions to the Formation and Identification of Cracks

The effect of different stress levels, corrosion, and welding were also studied. Table is a list of the specifications of each of the specimens at each conducted test.

Table 1- Specifications of test specimens for each test condition

Test type	Thickness(in)	Free Length(in)	Width(in)	Material	Center notch diameter(in)
Initial tests	1/8	8	1	ASTM A108	1/4
Stress level variation	1/8	8	1	ASTM A36	1/4
Corrosion	1/8	8	1	ASTM A36	No
Welding	1/8	8	1	ASTM A36	No
Thickness	1/4	8	1	ASTM A36	1/4

Variation in Stress Level

The effect of different stress levels on changes in the averaged MI was investigated and is shown in Figure 34. From this data, changing stress levels for the same specimens does not significantly alter the indication of the presence of the damage in VAM technique throughout the life of the specimen. Comparison of the extracted graphs in the highest and the lowest stress levels shows that the lower stress level will result in a delay in the failure prediction around 10% of the life of the specimen. However, since the life of the specimens in lower stress levels are longer, the portion of the remaining life in the normalized graphs once the percentage is converted to the number of fatigue cycles is still a large number that gives enough time for the maintenance (Figure 34 (b))
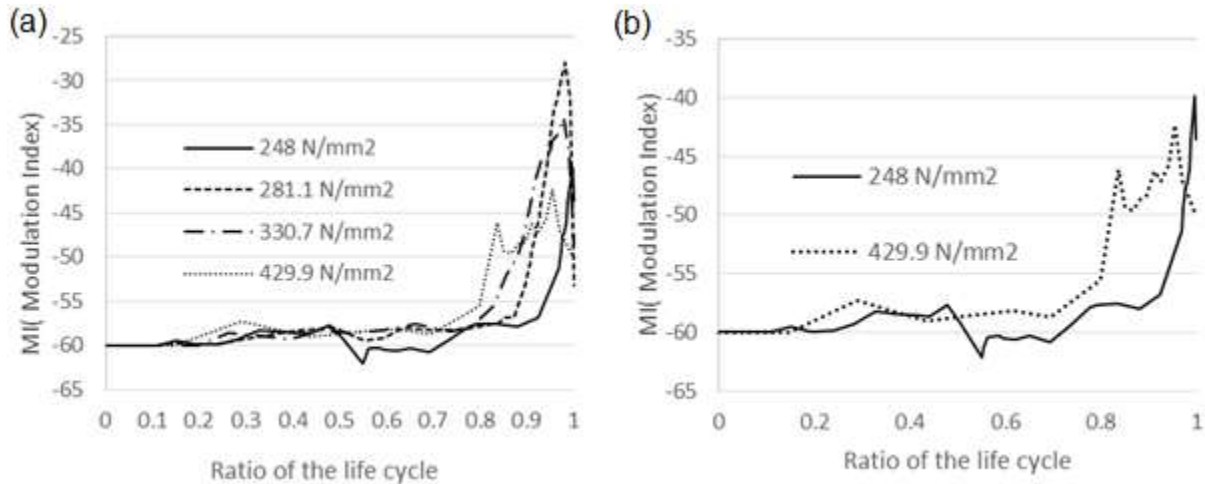

Figure 34. Trend of the modulation index vs ratio of the life cycles (effect of stress level variation): (a) in four stress levels, and (b) in maximum and minimum stress levels

38

Effect of Corrosion

The proposed NDT approach is also tested on corroded samples. Samples are corroded within an accelerated test in which they undergo cyclical wetting and drying process, as seen in Figure 35. The first cycle is a 5% saline solution spray for one hour. The following cycle is an hour of heat (produced by heat lamps to approximately 100° F) and UV irradiation to dry the specimens. These two cycles rotate one after another for 16 hours, producing 8 wetting and 8 drying cycles. Two different types of samples regarding the corrosion depth are created: type I is under exposure for two weeks and type II is under exposure for four weeks. The sample is covered with tape except for the middle part where the crack is intended to occur.

Figure 35. Corrosion equipment using UV at Rutgers University

It was observed that corroded samples differ from typical samples tested before in the modulation index progress during the fatigue life of the specimen. The steep slope that indicated damage in non- corroded samples is not observed. Instead a rather gradual increase of MI occurs during the fatigue cycles. The normalized MI-cycle number curves of type I and type II corroded samples are plotted in Figure 36 (b). Steady increase of MI during the fatigue life of the corroded samples can be correlated to the material degradation. However, not enough samples were available to provide statistical database for damage accumulation equations. To establish a baseline of damage indication by the VAM for failure prediction for corroded samples, more tests should be conducted in the future.
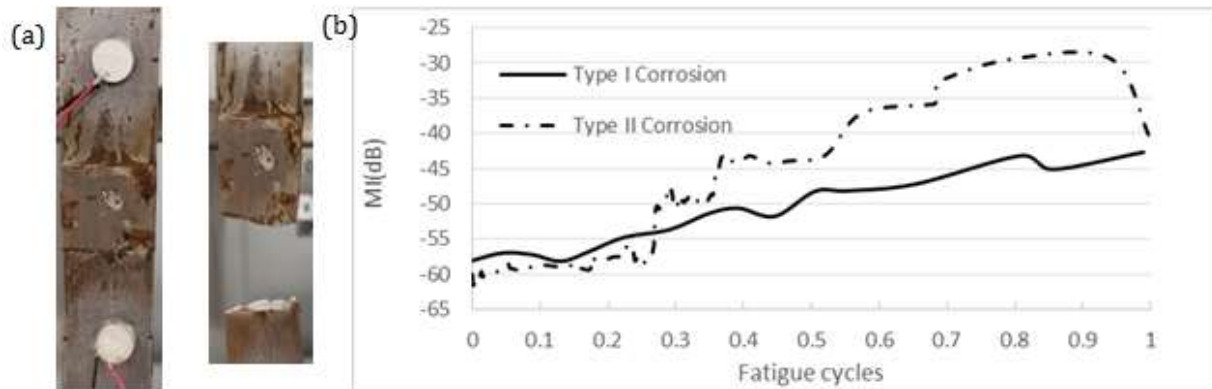
Figure 36. Corroded samples test results: (a) corroded sample type II specimen and fractured and (b) MI evolution in two type corroded specimens

Presence of Welding in the Member

To verify the potential applicability of the VAM method in bridge components welded specimens with specifications summarized in Table are subjected to tension only fatigue loading. Welded samples are prepared without the center notch with a groove in the center line (Figure 37.) The groove is filled with weld. The fatigue test load parameters are the same

The specimen is placed in the fatigue machine with the attached piezoelectric sensors as shown in Figure 38.   Figure 39 shows the evolving MI throughout the fatigue loading test. We observe that the MI increases to about -46 dB. The former non-welded specimens showed an MI increase up to -30 dB with a steep slope beginning after 70% of the life of the specimens. In the welded specimens, the steep slope occurs around 70% of their lifetimes as well.

Similar to the observed results in the regular initial test specimens, the steep increase of MI in welded and doubled thickness specimens also started as soon as 70-75% of life time has passed.
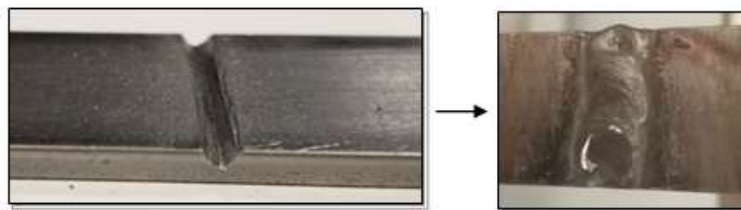
Figure 37. Welded specimen preparation
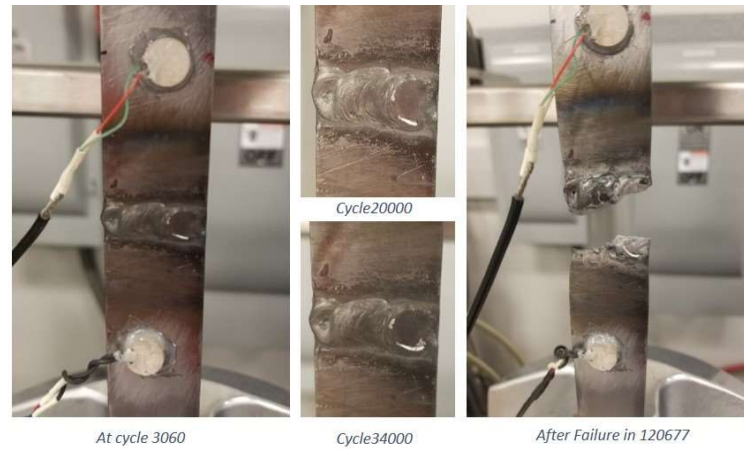
Figure 38. Welded specimen at different stages during the fatigue experiment
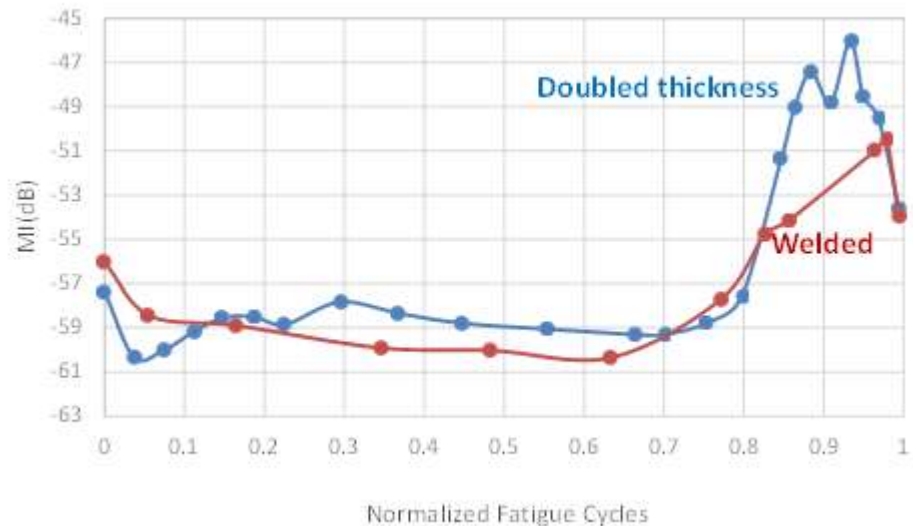
Figure 39. Modulation Index vs number of fatigue cycles ratio for doubled thickness and welding

Crack Detection Capability of VAM compared to UT and ET
Comparison between Ultrasonic Testing (UT), Eddy Current Testing (ET) and Vibro-Acoustic Modulation Methods provides information regarding sensitivity of these methods to fatigue cracks. The 1/8 inch-thick center hole specimen (as used in previous test series) is tested with 20 KN maximum tension load and 10 Hz cycling loading. Fatigue test had been conducted until the slope increase of Modulation Index (MI) was observed. The MI is measured in 5 kHz range sweeping carrier frequency with 100 Hz steps. In fact, the MI is averaged over 50 measured values. The range is selected in a flat portion of amplitude frequency response of the sample under test (SUT) to avoid the effect of distortions of frequency response. The increase in the MI is the indicator of defect in the sample via VAM. Figure 40 shows the MI-cycle number

41

curve in which two colored lines separates two consecutive test days. The test is stopped as soon as the MI increase observed. The sample is taken out of the fatigue machine. UT and ET equipment are used to investigate whether any sign of defect in the sample can be detected. Note that neither of the conventional tests is capable of identifying signs of defect in the sample. Hence, we concluded that Vibro- Acoustic Modulation Method is superior to existing technologies in regard to sensitivity of defect detection. When the crack is visible, both UT and ET are capable of crack detection.

Figure 40. Modulation Index vs Number of Fatigue cycles (tested with EC and UT)
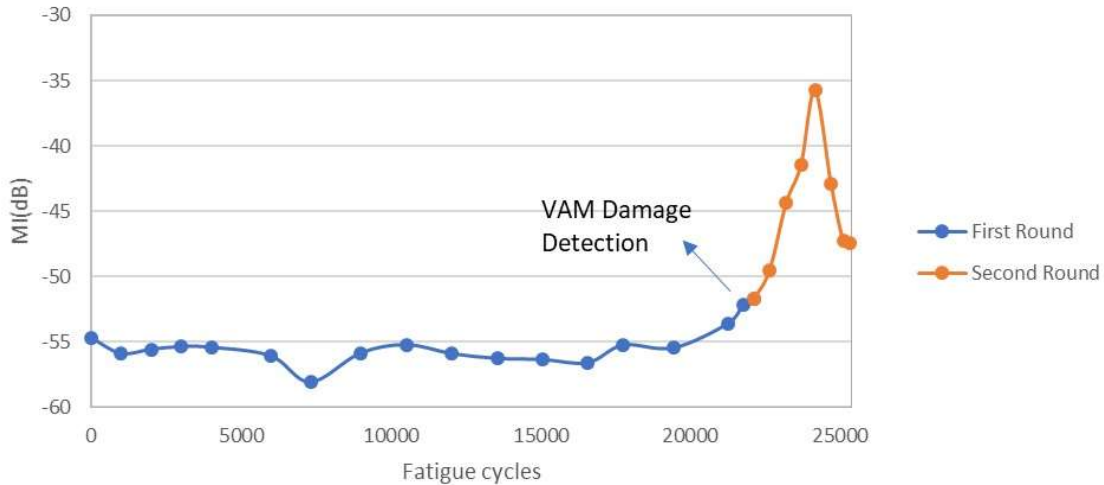
Continuous VAM, UT and ET Inspection

The test was repeated using a new sample with 10 in thickness, 1 in width and 1/8 in thickness is subjected to fatigue cycling loading to compare sensitivity of VAM, UT and ET to the fatigue defects. The cycling loading is 0 to 20 KN. The cycling loading introduced 10 Hz low frequency signal. The carrier signal would be modulated by this low frequency signal in presence of cracks. The MI evolution during fatigue experiment is recorded. This sample failed at cycle 50450 and the crack was visible at cycle 45921. The fatigue cycles are normalized to the fatigue life time of the specimen; therefore, the horizontal axis of Figure 41 shows values between 0 and 1. As it is indicated in Figure 41, the steep slope in the MI vs. Cycles is observed around 75% of the fatigue life of the specimen. Continuous monitoring of the sample with three approaches – VAM, UT and ET – show that VAM is the most sensitive to the structural defects.

When MI abrupt increase is observed during fatigue experiment, no observation of damage could be detected by UT and ET. The VAM, ET and UT methods could be able to predict the crack before it is observable. It should be mentioned that better sensitivity of VAM compared to UT and ET is not the only advantage of VAM with respect to UT and ET. The main advantage of VAM over UT and ET is its global inspection capability. Installment of a series of sensors on the sample will help to detect flaws remotely whereas the UT and ET need manual inspection of the component.

42
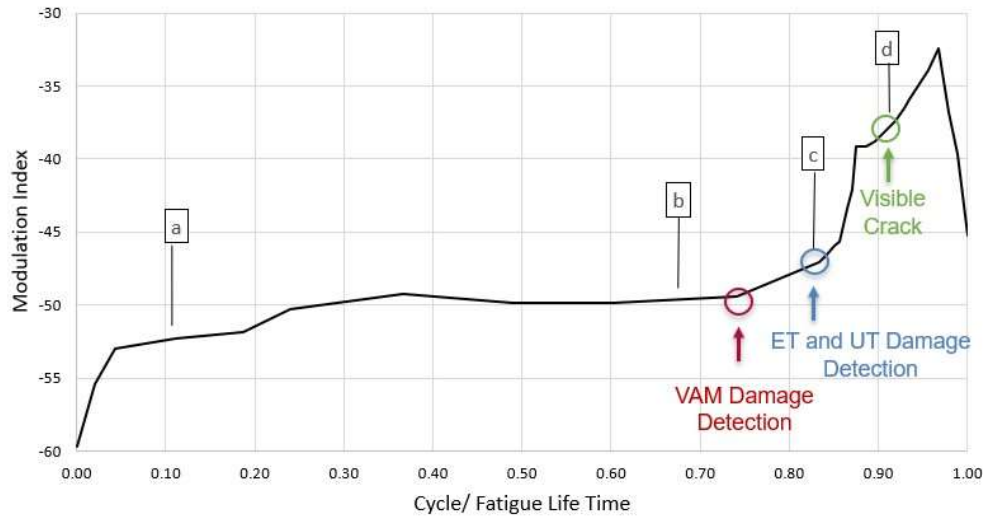
Figure 41. The sample is inspected by ET and UT at a) 11%, b) 68%, c) 83%, and d) 95% of its fatigue life time

Remaining Life Using Paris Law and Classical Fracture Mechanics

In order to estimate the remaining life of an element using classical mechanics, one would need 1) experimentally determined stress-concentration factors for the particular geometry of the element 2) the rate of the crack growth at a specified stress ratio, 3) initial crack length, 4) material strength. A calculation for the remaining life of one tested coupon is given in Appendix A. Data for the simple coupons have been taken from literature.

Unfortunately, such data is not readily available for actual connections and bridge elements. As such finite element analysis may be a good substitute to calculate fatigue strength. In this research, a finite-element analysis for A36 steel using MIDAS NFX for a test coupon shows the development of a crack at around 30,000 cycles. Finite elements will be very useful in the analysis of more complicated shapes.

Figure 42. Development of damage at 30,000 stress-reversals (Goodman correction)

CONCLUSIONS AND RECOMMENDATIONS

This study set out to investigate the applicability of the VAM technique in the field testing for critical bridge components made out of structural steel. The desired outcome would help us prevent disastrous collapse of bridges by estimation of the remaining fatigue life of the fracture critical members. Therefore, several fatigue tension only tests have been conducted on two types of steel material, ASTM A-36 and ASTM A-10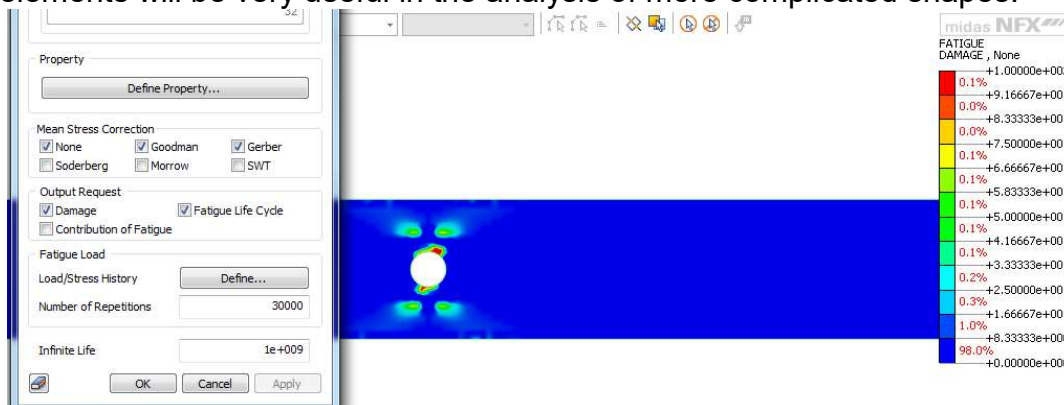8. As a result of these tests for the typical test specimens under similar condition, 20 to 30 percent of the life cycle damage precursor warning before failure was demonstrated. In this investigation, the following research goals had been met.

Using a Low Frequency Vibration as Modulating Frequency
- Preliminary tests of the VAM method using vibration in the natural frequency were conducted and the steel material degradation was successfully observed.
- Fatigue load cycling used for the measurements can successfully substitute resonance frequency generated by the shaker as a modulating frequency source.
- In the tests with typical specimens, consistency in the trends of MI is observed with respect to fatigue cycles per fatigue life time, meaning that gradual increase of the graph in the beginning changed to a steep slope in 70% to 80% of the fatigue life time of the specimen.
- The general applicability test of the VAM technique for thicker samples turned out successfully with start of the steep slope 25% to 30% before the actual failure occurred.

Amplitude and Frequency Modulation Significance in VAM Method
- The Vibro-Acoustic Modulation method reliably detects and monitors damage evolution from micro-defects to macro-cracks. Contact-type structural elements such as bolt connections and other structural components may create significant baseline nonlinearity, limiting VAM practical implementation. I hypothesized that fatigue damage may produce predominantly Frequency Modulation, while contact structural nonlinearities produce primarily Amplitude Modulation. If true, separating AM and FM may address the major deficiency of the VAM method.
- Structural contacts (as well as large cracks) exhibit AM, while initial stage of fatigue damage generates primarily FM. This is a very significant finding promising improved detection and characterization of damage evolution, which was demonstrated experimentally.

Algorithm Development for AM/FM Separation in VAM Method
- AM/FM separation using the traditional Hilbert Transform may not work for multipath propagation, which is common in practical settings. Therefore, two new AM/FM separation techniques, IQHS and SPHS algorithms, have been developed and validated both numerically and experimentally.
- The further investigation of IQHS and SPHS algorithms show that these algorithms can separate AM and FM components of VAM response during the fatigue experiments. However, both AM and FM components appear in the modulated signal, the AM is the dominant component of the output signal. Although modulation index of AM is higher than 10 times of MI of FM, both AM

and FM show increase during the fatigue experiment. The FM component could be a sign of crack formation in the presence of high nonlinearity due to the contact-type connections which makes MI reading impossible.
- Modulation phase is capable of predicting crack with more precision in earlier stage.

Effects of Corrosion and Welding
- The MI evolution in corroded samples does not comply with the warning of the crack existence at 70 to 80 percent of the fatigue life time. The investigation showed that a gradual increase in the MI during the life of the corroded specimens can contribute in a different way to the life cycle analysis.
- Welded and thicker samples show damage at remaining 25% to 30% of the fatigue life of the specimens.
- The VAM technique application in one of the samples was compared with the conventional NDT techniques of Ultrasonic Testing and Eddy Current Testing. The results revealed that the VAM technique was more sensitive to the presence of crack than these two conventional techniques.

Recommendations

Demodulation of the received signal from Vibro-Acoustic Modulation testing of the specimens shows preliminary frequency modulation dominance in micro-crack initiation and growth compared to prevalent amplitude modulation in contact-type macro-crack formation. These findings contribute in several ways to the application of this approach and pave the way for more research in this area for different samples with different geometries both in small and large scales. Considerably more empirical work needs to be done on variety of fatigue prone details in bridges both in small and actual scale to establish the VAM technique as an applicable method for life cycle analysis of bridges. The IQHS and SPHS algorithms could solve the problems towards practical implementation of the VAM method on existing structures. Therefore, a series of comprehensive tests should be performed on the real structures in the field to identify the effects of stress level, load type, geometry, bolts, corrosion, painting conditions, etc.

Resulting Publications

Detailed analyses of the subjects summarized in this report are found in two Ph.D. dissertations [57,58] and several conference and journal articles. [59,60,61]

IMPLEMENTATION AND TRAINING

An FN-Scan experimental system has been developed. The system is based on the breakthrough technique of "Nonlinear Vibro-Acoustic Modulation" which offers a highly sensitive testing process that may greatly enhance the current capabilities of structural Health Monitoring (SHM) and Non-Destructive Evaluation (NDE). During the research part of the project, a number of new procedures and algorithms have been developed and tested under laboratory conditions. The technique was proven successful in identifying damage accumulation before the development of visible cracks in small-scale steel samples. However, the technique was not tested for its ability to detect damage in large- or full-size structural components subjected to real-life conditions and loadings. Therefore, the major goal of the Implementation Plan is to use the FN-Scan system to conduct tests on large- and full- size structural components under real life conditions. Such tests are needed in order for the new technology to be developed further and be used outside the laboratory.

What is described here is a plan for further development of the FN-Scan system. The following three phases have been identified as critical to meet the objectives:

Phase 1: Large-Scale, Laboratory Testing of all developed algorithms on a number of large-scale bridge structural components. These tests will be conducted in a laboratory with the appropriate facilities capable of handling full-size components. One potentially suitable laboratory is the ATLSS Engineering Research Center in Lehigh University. The center has an active industrial testing program and they perform structural tests for bridge owners, consultants and manufactures. Stevens has been in contact with the center for a possible collaboration on large-scale testing of bridge connections. The FN-Scan system developed herein will be used and further developed to identify damage on the large components. The enhanced system will then be ready for further testing and development in the field.

Phase. 2: Field test on a steel bridge using bridge ambient vibrations as one of the input signal. This has never been done and it will be a truly pioneering step toward real life implementation of the VAM technology. This will be a critical phase allowing real life data collection, verification and modifications of the developed algorithms. If successful, the algorithms and procedures will be finalized and formulated for software implementation into a final system.

Phase 3: Development of an end-user-friendly system that can be taken to the field. The prototype system, used during Phase 1 and 2 is the experimental data-collection and proof-of-concept system. Once the developed technology is verified and finalize, an end-user- friendly system will be developed and prototyped. At this phase, the collaboration with an industrial partner will be the key to successful transition and implementation to the real world.

REFERENCES

1. Chudnovsky, A. Intrinsic Time and Aging, (with C.P. Bosnyak), in *Handbook of Modern Sensors*, 2nd Edition by J. Fraden, American Institute of Physics Press, Woodbury, NY, 1996.
2. The AASHTO Bridge Element Inspection Guide Manual, American Association of State Highway and Transportation Officials, First Edition 2013 (with revisions 2015).
3. NJDOT Evaluation and Bridge Management, Prepared by Structural Evaluation & Bridge Management, 2014 (with revisions 2015).
4. AASHTOWare^{TM} Bridge Management software (BrM) (formerly PONTIS), http://aashtowarebridge.com
5. AASHTO. 1990. Guide Specifications for Fatigue Evaluation of Existing Steel Bridges. American Association of State Highway and Transportation Officials, Washington, DC.
6. AASHTO. 2010. AASHTO LRFD Bridge Design Specifications, Fifth Edition. American Association of State Highway and Transportation Officials, Washington, DC.
7. AASHTO. The Manual for Bridge Evaluation (MBE), Second Edition, 2011.
8. NCHRP Report 721, Fatigue Evaluation of Steel Bridges, Transportation Research Board, Washington, DC, 2012.
9. NCHRP 354 Report, Inspection and Management of Bridges with Fracture-Critical Details, Transportation Research Board, Washington, DC, 2005.
10. Donskoy DM, Sutin AM. Vibro-acoustic modulation nondestructive technique. *Journal of Intelligent Material Systems and Structures* 1999 **9**:765–771.
11. Donskoy DM, Sutin AM, Ekimov A. Nonlinear acoustic interaction on contact interfaces and its use for nondestructive testing. *NDT International* 2001 **34**:231–238.
12. I. Solodov, D. Doring, and G. Busse, "New opportunities for NDT using non-̈linear interaction of elastic waves with defects," *Strojniski Vestnik-Journal oḟ Mechanical Engineering*, vol. 57, no. 3, pp. 169–182, 2011.
13. K. A. Van Den Abeele, P. A. Johnson, and A. Sutin, "Nonlinear elastic wave spectroscopy (NEWS) techniques to discern material damage, part I: nonlinear wave modulation spectroscopy (NWMS)," *Research in Nondestructive Evaluation*, vol. 12, no. 1, pp. 17–30, 2000.
14. A. Klepka, W. Staszewski, R. Jenal, M. Szwedo, J. Iwaniec, and T. Uhl, "Nonlinear acoustics for fatigue crack detection experimental investigations of vibro-acoustic wave modulations," *Structural Health Monitoring*, vol. 11, no. 2, pp. 197–211, 2012.
15. W. De Lima and M. Hamilton, "Finite-amplitude waves in isotropic elastic plates," *Journal of Sound and Vibration*, vol. 265, no. 4, pp. 819–839, 2003.
16. A. Hikata and C. Elbaum, "Generation of ultrasonic second and third harmonics due to dislocations. I," *Physical Review*, vol. 144, pp. 469–477, Apr 1966.
17. A. Zagrai, D. Donskoy, A. Chudnovsky, E. Golovin, and V. S. Agarwala, "Micro/meso scale fatigue damage accumulation monitoring using nonlinear acoustic vibro-modulation measurements," in *Nondestructive Evaualation for*

Health Monitoring and Diagnostics. International Society for Optics and Photonics, 2006, Art no. 617506

18. J. H. Cantrell and W. T. Yost, "Nonlinear ultrasonic characterization of fatigue microstructures," *International Journal of Fatigue*, vol. 23, pp. 487–490, 2001.

19. V. Zaitsev, V. Nazarov, V. Gusev, and B. Castagnede, "Novel nonlinearmodulation acoustic technique for crack detection," *NDT & E International*, vol. 39, no. 3, pp. 184–194, 2006.

20. D. M. Donskoy, "Nonlinear acoustic methods," in *Encyclopedia of Structural Health Monitoring*, C. Boller, F. K. Chang, and Y. Fujino, Eds. Wiley Online Library, 2009, ch. 15, pp. 321–332.

21. C. Vanhille and C. Campos-Pozuelo, "A numerical formulation for nonlinear ultrasonic waves propagation in fluids," *Ultrasonics*, vol. 42, no. 10, pp. 1123–1128, 2004.

22. J. Federlein, T. Postert, S. Meves, S. Weber, H. Przuntek, and T. Buttner,¨ "Ultrasonic evaluation of pathological brain perfusion in acute stroke using second harmonic imaging," *Journal of Neurology, Neurosurgery & Psychiatry*, vol. 69, no. 5, pp. 616 LP – 622, 2000.

23. A. Anvari, F. Forsberg, and A. E. Samir, "A primer on the physical principles of tissue harmonic imaging," *RadioGraphics*, 2015.

24. V. M. Mukhortov, S. V. Biryukov, Y. I. Golovko, G. Y. Karapet'yan, S. I. Masychev, and V. M. Mukhortov, "Surface acoustic waves in thin films of barium strontium titanate on magnesium oxide substrates," *Technical Physics Letters*, vol. 37, no. 3, p. 207, 2011.

25. M. Deng and J. Pei, "Assessment of accumulated fatigue damage in solid plates using nonlinear Lamb wave approach," *Applied Physics Letters*, vol. 90, no. 12, mar 2007, Art no. 121902.

26. M. Hasanian and C. J. Lissenden, "Second order harmonic guided wave mutual interactions in plate: Vector analysis, numerical simulation, and experimental results," *Journal of Applied Physics*, vol. 122, no. 8, 2017, Art no. 84901.

27. H. Xiaobin, L. Yuan, L. Peisong, and X. Weiying, "Interfacial adhesionstrength detection of structural silicone sealant for hidden framesupported glass curtain wall based on nonlinear ultrasonic Lamb wave," *Journal of Aerospace Engineering*, vol. 31, no. 5, p. 4018047, sep 2018. [Online]. Available: https://doi.org/10.1061/(ASCE)AS.1943-5525.0000870

28. M. Hasanian and C. J. Lissenden, "Directional nonlinear guided wave mixing: Case study of counter-propagating shear horizontal waves," *AIP Conference Proceedings*, vol. 1949, no. 1, 2018, Art no. 70002.

29. A. Ouahabi, M. Thomas, and A. Lakis, "Detection of damage in beams and composite plates by harmonic excitation and time-frequency analysis," in *Proceedings of the 3rd European Workshop on Structural Health Monitoring, Granada, Spain*, 2006, pp. 775–782.

30. J. H. Cantrell, "Dependence of microelastic-plastic nonlinearity of martensitic stainless steel on fatigue damage accumulation," *Journal of Applied Physics*, vol. 100, no. 6, 2006, Art no. 063508.

31. J. L. Rose, *Ultrasonic guided waves in solid media*. Cambridge: Cambridge University Press, 2014.

32. H. Hu, W. Staszewski, N. Hu, R. Jenal, and G. Qin, "Crack detection using nonlinear acoustics and piezoceramic transducers-instantaneous amplitude and frequency analysis," *Smart Materials and Structures*, vol. 19, no. 6, 2010, Art no. 065017.

33. T. Ooijevaar, M. Rogge, R. Loendersloot, L. Warnet, R. Akkerman, and T. Tinga, "Vibro-acoustic modulation-based damage identification in a composite skin-stiffener structure," *Structural Health Monitoring*, vol. 15, no. 4, pp. 458 – 472, 2016.

34. J. Y. Kim, V. Yakovlev, and S. Rokhlin, "Parametric modulation mechanism of surface acoustic wave on a partially closed crack," *Applied Physics Letters*, vol. 82, no. 19, pp. 3203–3205, 2003.

35. J. Y. Kim, Y. VA., and R. SI., "Surface acoustic wave modulation on a partially closed fatigue crack," *The Journal of the Acoustical Society of America*, vol. 115, no. 5, pp. 1961–1972, 2004.

36. D. M. Donskoy and A. M. Sutin, "Method and apparatus for acoustic detection and location of defects in structures or ice on structures," U.S. Patent 6 301 967, 2001.

37. D. Donskoy, A. Ekimov, E. Luzzato, J. L. Lottiaux, S. Stoupin, and A. Zagrai, "N-scan: new vibromodulation system for detection and monitoring of cracks and other contact-type defects," in *Smart Systems and Nondestructive Evaluation for Civil Infrastructures*, vol. 5057, 2003.

38. E. Ballad, S. Y. Vezirov, K. Pfleiderer, I. Y. Solodov, and G. Busse, "Nonlinear modulation technique for NDE with air-coupled ultrasound," *Ultrasonics*, vol. 42, no. 1, pp. 1031–1036, 2004.

39. H. J. Lim, B. Song, B. Park, and H. Sohn, "Noncontact fatigue crack visualization using nonlinear ultrasonic modulation," *NDT & E International*, vol. 73, pp. 8–14, 2015.

40. C. Hedberg, S. Andersson, K. Haller, and S.-E. Hallbratt, "Non-contact nonlinear ultrasound scan of a cfrp plate with manufactured damages," in *Interntational Workshop of Structural Health Monitoring*. Stanford University, Sept 12-14, 2013.

41. J.Zakrzewski, N.Chigarev, V.Tournat, and V.Gusev,"Combined photoacoustic–acoustic technique for crack imaging," *International Journal of Thermophysics*, vol. 31, no. 1, pp. 199–207, 2010.

42. Y. Zhang, V. Tournat, O. Abraham, O. Durand, S. Letourneur, A. Le Duff, and B. Lascoup, "Nonlinear mixing of ultrasonic coda waves with lower frequency-swept pump waves for a global detection of defects in multiple scattering media," *Journal of Applied Physics*, vol. 113, no. 6, 2013, Art no. 064905.

43. S. Mezil, N. Chigarev, V. Tournat, and V. Gusev, "All-optical probing of the nonlinear acoustics of a crack," *Optics Letters*, vol. 36, no. 17, pp. 3449– 3451, 2011.

44. C. Y. Ni, N. Chigarev, V. Tournat, N. Delorme, Z. H. Shen, and V. E. Gusev, "Probing of laser-induced crack modulation by laser-monitored surface waves and surface skimming bulk waves," *The Journal of the Acoustical Society of America*, vol. 131, no. 3, pp. 250–255, 2012.

45. G. M. Whitesides, J. K. Kriebel, and B. T. Mayers, "Self-assembly and nanostructured materials," *Nanoscale Assembly*, no. 9, pp. 217–239, 2005.
46. M. Shishehbor and P. D. Zavattieri, "Effects of interface properties on the mechanical properties of bio-inspired cellulose nanocrystal (CNC)-based materials," *Journal of the Mechanics and Physics of Solids*, vol. 124, pp. 871–896, 2019.
47. H. Bhadeshia, "The first bulk nanostructured metal," *Science and Technology of Advanced Materials*, vol. 14, no. 1, 2013, Art no. 014202.
48. D. M. Jacobson and G. Humpston, *Principles of Brazing*. Materials Park, OH, USA: ASM International, 2005.
49. Y. Kim, H. J. Lim, and H. Sohn, "Nonlinear ultrasonic modulation based failure warning for aluminum plates subject to fatigue loading," *International Journal of Fatigue*, vol. 114, pp. 130–137, 2018.
50. R. B. Jenal and W. J. Staszewski, "Crack detection in glass plates using nonlinear acoustics with low-profile piezoceramic transducers," in *Health Monitoring of Structural and Biological Systems 2010*, vol. 7650. Proceedingas of SPIE, 2010, Art no. 765030.
51. A. Klepka, L. Pieczonka, W. Staszewski, and F. Aymerich, "Impact damage detection in laminated composites by non-linear vibro-acoustic wave modulations," *Composites Part B: Engineering*, vol. 65, pp. 99–108, oct 2014.
52. P. Duffour, M. Morbidini, and P. Cawley, "A study of the vibro-acoustic modulation technique for the detection of cracks in metals," *The Journal of the Acoustical Society of America*, vol. 119, no. 3, pp. 1463–1475, 2006.
53. P. B. Dao, A. Klepka, Ł. Pieczonka, F. Aymerich, and W. J. Staszewski, "Impact damage detection in smart composites using nonlinear acoustics - cointegration analysis for removal of undesired load effect," *Smart Materials and Structures*, vol. 26, no. 3, p. 035012, 2017.
54. L. Pieczonka, L. Zietek, A. Klepka, W. J. Staszewski, F. Aymerich, and T. Uhl, "Damage imaging in composites using nonlinear vibro-acoustic wave modulations," *Structural Control and Health Monitoring*, vol. 25, no. 2, 2018.
55. J. A. Collins, *Failure of Materials in Mechanical Design: Analysis, Prediction, Prevention*. New York, USA: John Wiley & Sons, 1993.
56. R. Dreyfuss, "Standard practice for conducting force controlled constant amplitude axial fatigue tests of metallic materials," in *Annual Book of ASTM*. American Society for Testing and Materials, 2003, pp. 515–519.
57. M. Rameznai Goldyani, "*Enhancement of Joining Method and Damage Detection Methodology in Structural Materials*" Ph.D. Dissertation, Stevens Institute of Technology, Hoboken, N.J., 2018.
58. B. Golchinfar, "*Health Monitoring of Structural Materials with Innovative Nondestructive Testing Method*," Ph.D. Dissertation, Stevens Institute of Technology, Hoboken, N.J., 2019.
59. Donskoy, D.M.; Ramezani, M. *Separation of amplitude and frequency modulations in Vibro-Acoustic Modulation Nondestructive Testing Method*. Proc. Meet. Acoust. 2018, 34, 045002.

60. Donskoy, D.; Golchinfar, B.; Ramezani, M.; Rutner, M.; Hassiotis, S. *Vibro-acoustic amplitude and frequency modulations during fatigue damage evolution*. In Proceedings of the AIP Conference Proceedings; 2019; Vol. 2102, p. 040004.

61. Ramezani, M.G.; Golchinfar, B.; Donskoy, D.; Hassiotis, S.; Venkiteela, G. *Steel Material Degradation Assessment Via Vibro-Acoustic Modulation* Technique. Transp. Res. Rec. J. Transp. Res. Board 2019, 036119811983827.

62. J. A. Collins, *Failure of materials in mechanical design : analysis, prediction, prevention*, 2. ed. ed. (Wiley-Interscience publication). New York :: Wiley (in English), 1993.

63. H. Tada, P. C. Paris, and G. R. Irwin, "The stress analysis of cracks," *Handbook, Del Research Corporation,* 1973.

64. R. A. DeMarte, "Analysis of Fatigue Crack Propagation in Welded Steels," 2016

APPENDIX

Using Paris Law to estimate remaining life-Sample Calculations

In this section the crack size is determined using Paris Law. The theoretical approach was taken to estimate the approximate crack size at the time the VAM technique detects the crack. Paris Law provides the number of the remaining fatigue cycles to the failure in case a series of parameters are known Input parameters needed are: initial crack size, critical crack size, type of material, and stress intensity factor. In this case, to be able to estimate the remaining number of cycles to the failure, crack size has to be known. In this investigation, utilizing the conducted tests information, with a backward approach, crack size can be determined and used as a reference for the rest of the tests. For the purpose of life prediction of our current sample, a step by step procedure using Paris law is conducted.[62]

To be able to extract the value of the desired parameters to use as inputs in Paris law, material properties of the specimen and the geometry of the samples in the experimental tests are described in Table A1 and A2.

Table A1- Required geometry specifications of the current sample

Width (W) (in)	1
Gauge Length (L) (in)	8
Load type	Tensile (Fluctuating)
Max load (kN)	20
Max Stress level (N/mm^2)	330
Min load (kN)	0
Min Stress level (N/mm^2)	0
Initial crack length (a_0) (m)	0.0015
Averaged number of cycles to the failure	53500

Table A2- Material properties of the current sample.

Structural Steel		
Yield Strength (σ_{yp})	36 ksi	250 MPa
Ultimate Tensile Strength	69ksi	480 MPa
Plane Strain Fracture Toughness (K$_{IC}$)		115 MPa√m
Fatigue Strength	29ksi	200 MPa
Module of Elasticity (E)	27000ksi	190GPa

The average number of cycles to the failure is also mentioned in Table A1 to be used in the integration over Paris Law given in Equation (A.1) that is used to calculate crack size once the crack is detected by VAM.

$$\frac{da}{dN} = C(\Delta K)^n \tag{A.1}$$

where a is the crack length, and $\frac{da}{dN}$ is the crack growth rate. C and n are constants that depend on the material, environment and stress ratio. ΔK is the range of the stress intensity factor during the fatigue cycle calculated using Equation (A.2.)

$$\Delta K = C_I \Delta\sigma\sqrt{\pi a} \tag{A.2}$$

To calculate ΔK , C_I has to be determined first This parameter is related to the geometry and type of loading that is exposed to the specimen. C_I in Figure A1 is introduced as $F(\frac{a}{b},\frac{R}{b},\frac{h}{b})$ in which b is half of the width of the specimen. R is the radius of the center notch and h is half of the gauge length of the specimen. $\Delta\sigma$ is the difference in the applied stress to the specimen.
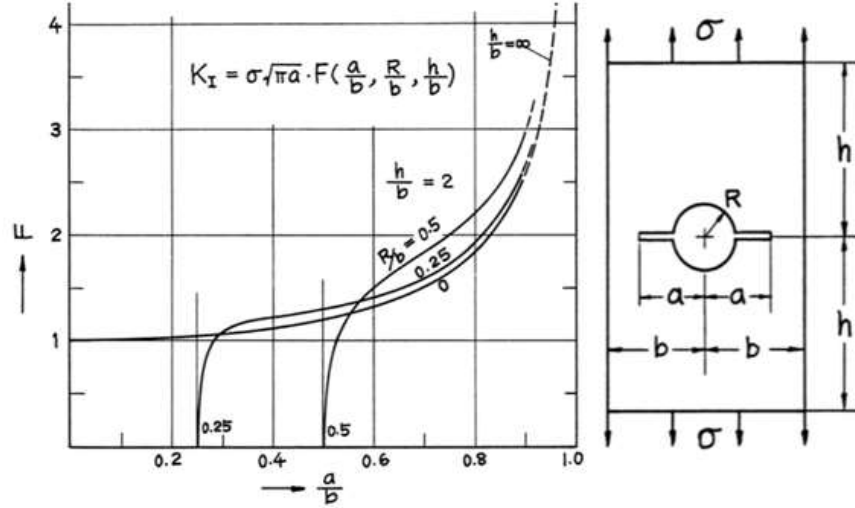

Figure A1. Experimental graphs for determining K$_I$ and C$_I$ [63]

In Figure A1 the corresponding graph for calculating C_I for the specific geometry and loading of the current testing specimen is shown.[63] To be able to extract C_I and K$_I$ using experimental graph in Figure A1 the parameters in Table A3 are calculated as follows: a=R+a$_o$ =0.03175+0.0015=0.03325 Here, a_0 is the assumed initial crack size.

Table A3- Required parameters to extract C$_I$ and K$_I$.

	c	b	h	R	h/b	a/b	R/b
Units in meters	0.3325	0.127	1.016	0.03175	8	0.26	0.29

According to the calculated numbers, C_I that is $F(\frac{a}{b},\frac{R}{b},\frac{h}{b})$ in Figure (A1) is equal to 1.2. C and n in Equations(A1) and (A2) are related to the material properties, applied stress level ratio ($R = \frac{\sigma_{min}}{\sigma_{max}}$) and loading frequency.

As seen in Figure (A2), for 10 Hz frequency loading of ASTM A36 and R=0.05, $C = 9 \times 10^{-13}$ and $n = 3.617$. Therefore, Paris Law in this case would be in the form of Equation (A3.)

$$\frac{da}{dN} = 9 \times 10^{-13} \times (1.2\Delta\sigma\sqrt{\pi a})^{3.617} \tag{A.3}$$

$$\Delta\sigma = \sigma_{max} - \sigma_{min}= 330 \text{ Mpa- } 0=330 \text{ Mpa} \tag{A.4}$$

Now the only unknown would be the crack size using the number of cycles to the failure. Hence, we can rewrite Equation (A3) in the form of Equation (A5) to be able to integrate
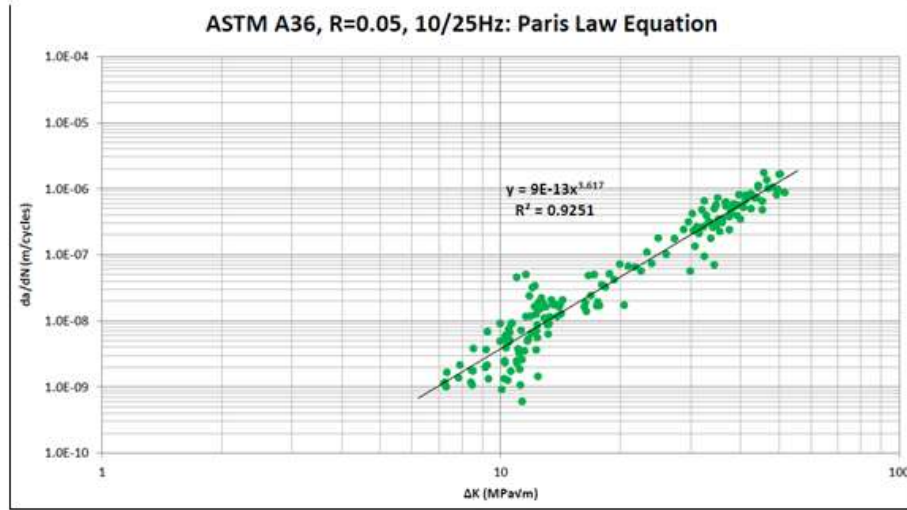
and calculate the desired crack size.

Figure A2. Crack growth rate data and Paris equation for ASTM A36 at stress ratio R = 0.05 with a test frequency of 10 and 25 Hz[64]

$$\frac{da}{a^{\frac{3.617}{2}}} = 9 \times 10^{-13} \times (1.2 \times 330 \times \sqrt{\pi})^{3.617} \, dN \tag{A.5}$$

Assuming that the initial crack size is $a_0 = 0.0015m$ and integrating both sides we can estimate the critical crack size. When N=0 with known N_f (Average number of cycles to the failure) the critical crack size will be estimated using equation (A6).

$$\int_{a_0=0.0015}^{a_f} \frac{da}{a^{\frac{3.617}{2}}} = \int_{0}^{53500} 9 \times 10^{-13} \times (1.2 \times 330 \times \sqrt{\pi})^{3.617} \, dN \tag{A.6}$$

Performing the integration using the MATLAB code gives $a_{cr} = 0.0032m$ as output
To be able to estimate the size of the crack that leads to the failure at the time VAM technique predicts its existence (a_p), number of cycles at which the steep slope starts will be used in addition to the critical size of the crack and number of cycles to the failure. The same code gives us the desired crack size.

$$\int_{a_p}^{a_f=0.0032} \frac{da}{a^{\frac{3.617}{2}}} = \int_{42900}^{53500} 9 \times 10^{-1} \times (1.2 \times 330 \times \sqrt{\pi})^{3.617} \, dN$$

Therefore, size of the crack at which VAM technique predicts is equal to 0.0027 m theoretically.

As a result of these calculations, utilizing a MATLAB code with parameterized Paris Law, the approximate critical crack size in the current specific testing sample is calculated. As inputs of the equation, the average number of cycles to the failure (53500) from the conducted tests in the lab was utilized.
The above calculations have to be done for the most critical elements of the structure for which we need the remaining life.

Stevens Institute of Technology

Castle Point on Hudson, Hoboken, NJ 07030

FN-SCAN® User's Guide

Experimental
Nonlinear Vibro-Modulation Testing System

Table of Contents

1. GENERAL INFORMATION

1.1 . General Description

The FN-SCAN® is an **experimenta**l portable nondestructive Structural health Monitoring (SHM) and NonDestructive Testing and Evaluation (NDT&E) system utilizing patented (U.S.Patent # 6,301,967 and other patent pending) Vibro-Modulation Testing technique (VMT). VMT allows for inspection and monitoring of structural integrity of metal, non-metal, and composite materials and structures, indicating the presence of contact-type defects such as cracks, debondings, delaminations, etc. This technique employs effect of nonlinear interaction of ultrasound (high frequency) and vibration (low frequency) in the presence of defects. Vibration changes contact area within the defect effectively modulating phase and amplitude of an ultrasonic signal passing through this varying contact interface. The major advantages of VMT include:

- Material independence
- Applicability to structures with complicated geometry
- Real time processing
- Interface with simple data output for pass/failed inspection

In the present configuration FN-SCAN® does not allow for localization of the defect; it is only indicates its presence and severity or absence.

1.2. Safety and Use

WARNING: F**N-SCAN® is an experimental system and supposed to be used ONLY for experimental validation of VMT. FN-SCAN® should not be used for actual inspections without proper certification.**

WARNING: Dangerous voltages, capable of causing death, are present in this electronic system. Use extreme caution whenever the instrument covers are removed.

The FN-SCAN® system components such as power amplifier and Digital Data Acquisition (DAQ) should only be connected via a three-wire power cord to an AC power source 220V having a line frequency of 60 or 50 Hz. Always use an outlet which has a properly connected protective ground.

Operating
The FN-SCAN® system can be operated outdoors if protected from the elements.
The system must not be turned on until all cables are connected. Make sure that all cables are connected properly and firmly. Protect all cables from mechanical damage.

Installing other components
Installing any other hardware or software components to the FN-SCAN® system which are not part of it as this is likely to damage the system.

2. SYSTEM DESCRIPTION: Configuration, Connections, and Installation

FN-SCAN® system consists of the following major components:

- System control, signal generation, processing, and storage housed in Ruggedized laptop computer (Panasonic Toughbook 54 Prime 14" Core i5 7300U 8 GB RAM) with proprietary   FN-SCAN® v4.0 software
- Ultrasonic Power Amplifier: Trek, Inc.2100HF-L-CE
- Data Acquisition USB board: National Instrument NI 6366
- Two ultrasonic transducers: Mistras, F15A, 100 -450 kHz
- Ultrasonic preamplifier/filter: Mistras 0/20/40 dB single-ended/differential AST preamplifier with a 2/4/6 series filter
- 3D accelerometer: Digi-Key, model 4030-002-120

FN-SCAN® connection diagram is shown in the Fig.2.1
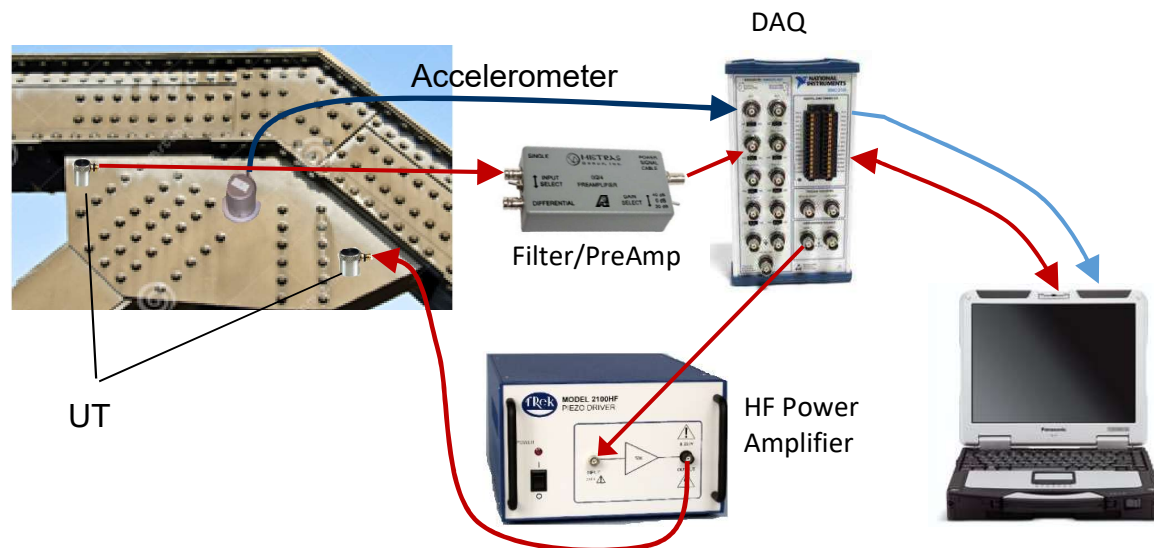
Fig.2.1. **FN-SCAN®** system components and connection diagram

Accelerometer and UT transducers Installation.

Accelerometer and transducers must be install to enable good acoustic coupling with structure under test. Accelerometer can be attached to the structure using screws or magnets. Special care should take for installation of the UT transducers. Besides good acoustic coupling, the interface

between the transducers and the surface of the structure should not introduce contact-type nonlinearity, i.e. should be no dry contact between transducers and the surface. The best coupling without nonlinearity is glue (such as fast setting epoxy glue) to the exposed metal surface of the structure (paint must be removed).

3. SYSTEM OPERATION

All operation of the system and all its components are fully controlled via FN-SCAN® interface software. FN-SCAN® has four mode of operations and respective displays: Oscilloscope, Spectrum Analyzing (SA) mode, N-Scan and FN-Scan modes.

3.1 Start-up

To make measurements with the FN-SCAN® proceed as follows:

1. Attach accelerometer and UT transducers to the structure under test.
2. Connect the system according to the diagram in Fig.2.1.
3. Turn ON all system devices.
4. On the laptop Desktop screen double-click the short-cut icon FN-Scan.

The FN-SCAN® program starts and the Application Display, Fig.3.1, appears. The display has soft buttons and control tabs, which set and control FN-SCAN® system operation.
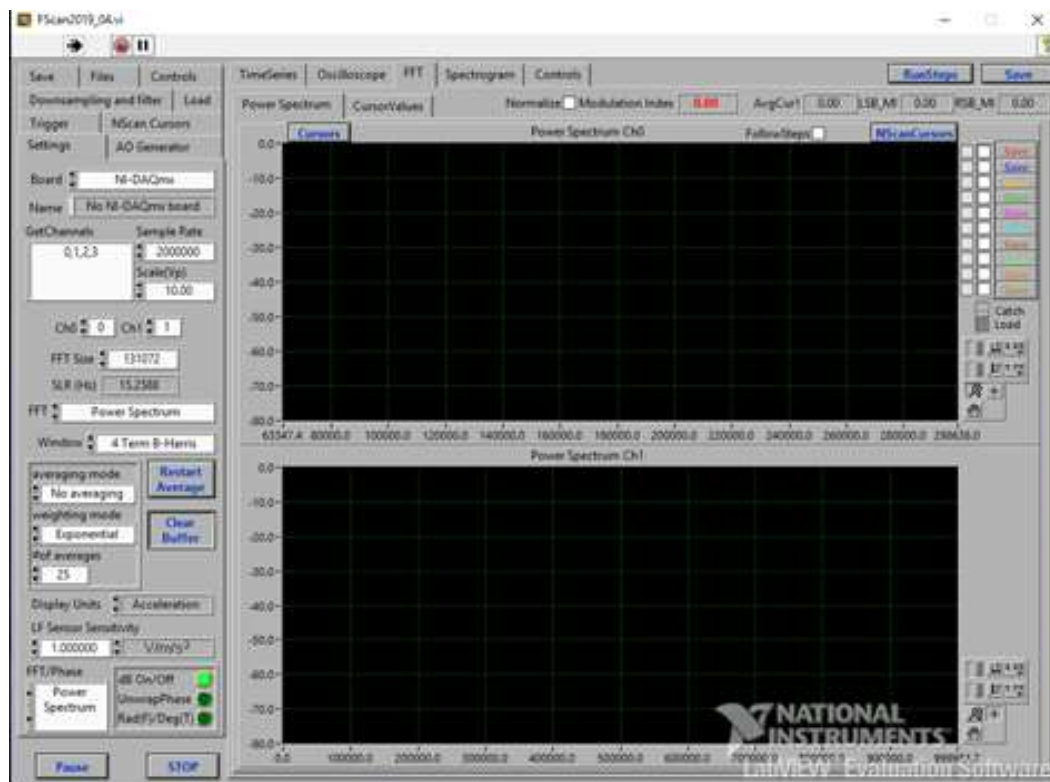
Fig.3.1. FN-SCAN® Application Display

3.2. Application Display

FN-SCAN® has a multiple displays [TimeSeries Oscilloscope | FFT | Spectrogram | Controls |] which can be switch on using tabs above the signal screens.

3.2.1. Oscilloscope Mode

There are two ocsilloscope screens activated by tabs **TimeSeries** and **Oscilloscope** situated above the signal screen.

- TimeSeries shows an oscillograms of the acquired signals in the DAQ buffer.

- Oscilloscope shows oscillograms of the acquired signal in predefined time interval defined by the "ScopeTime" box situated to left of the screen, Fig.3.2.2.

- TimeSeries shows an oscillogram of the acquired signals in the DAQ buffer.

- Oscilloscope shows oscillograms of the acquired signal in predefined time interval defined by the "ScopeTime" box situated to left of the screen, Fig.3.2.2.
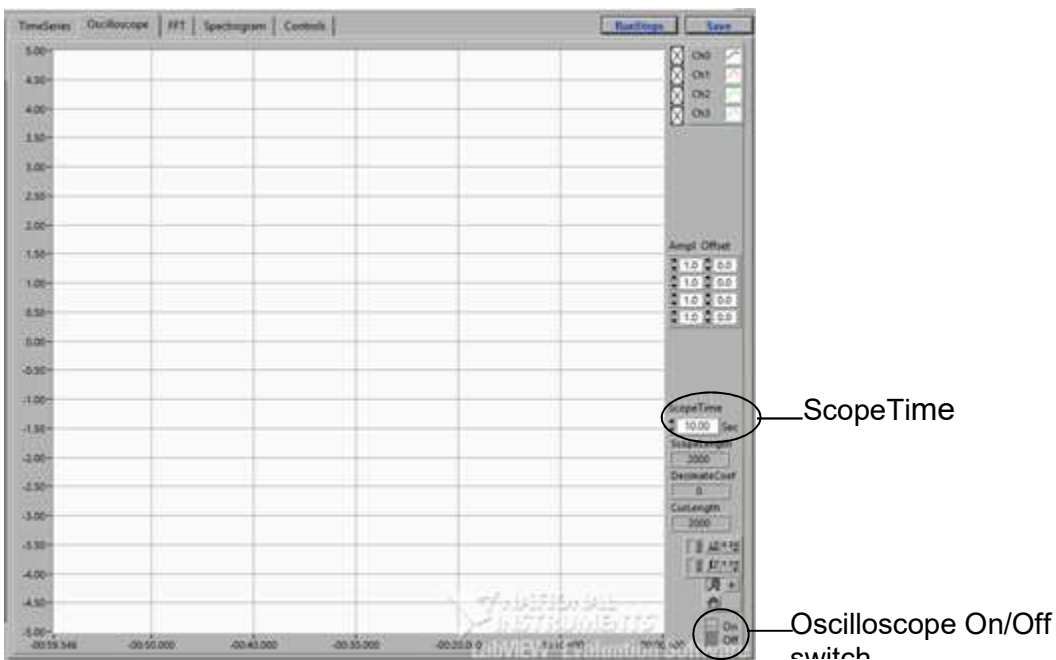
Fig.3.2.2. Oscilloscope display.

3.2.2. Spectrum Analyzing (SA) Mode

SA mode is an auxiliary mode for analyzing vibration frequency response of a structure under test. Fig.3.2.3, shows **Power Spectrum** of received signals as well as post processed data such as Modulation Indexes vs Frequency Scan using tab **CursorValues**

The displayed spectrum could be zoomed in or out using [icons] soft buttons. The button [icon] can be used to undo previously changed zoom (undo only the last change). The axis scales can also be changed by clicking on first/last scale number and manually typing a desirable number.

Standard spectrum averaging (arithmetic, exponential, and peak) can also be used in SA mode by choosing the respective options in the dial boxes: [No Average] and [Number of averaging | 100] located in tab **Average** in **Settings** panel, Fig. 3.2.3. LF averaging cannot be used if N-Scan mode is activated.

The displayed spectrum can be captured and saved as a separate Excel file by using soft button **Save**.
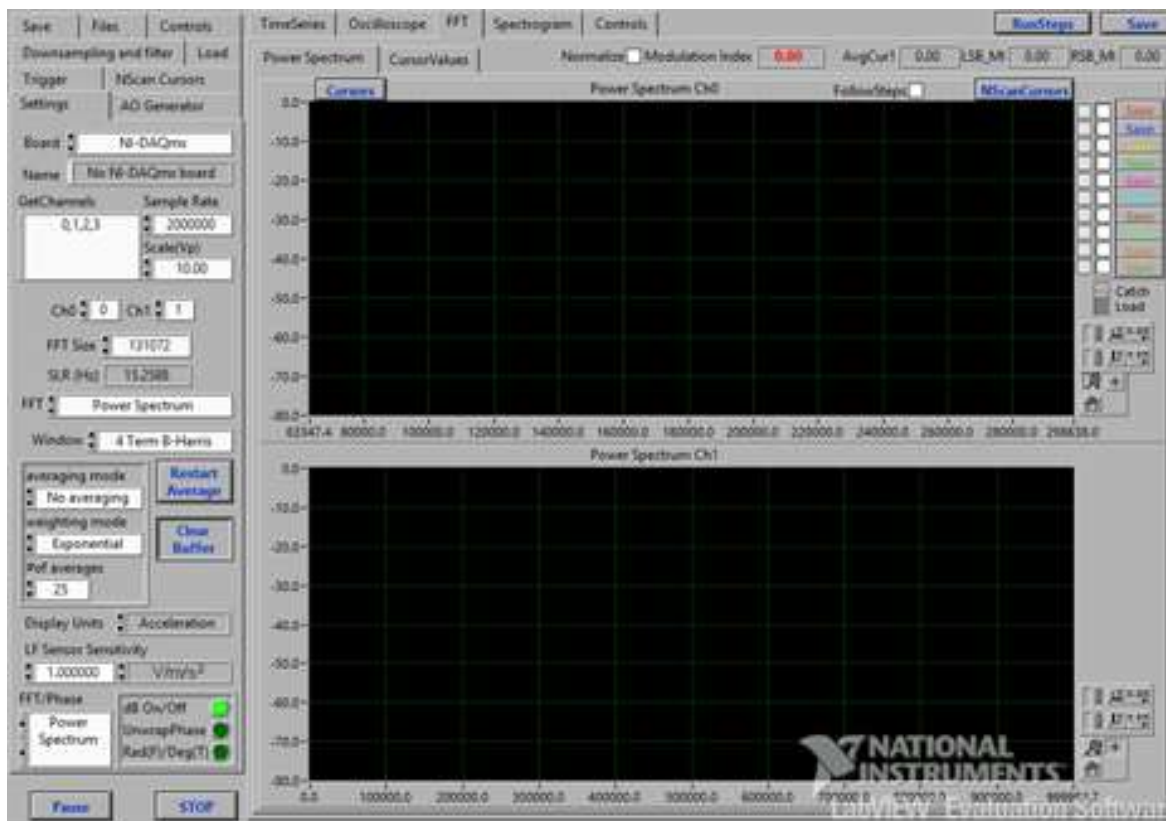

Fig.3.2.3. Power Spectrum Display.

As any spectrum analyzer, FN-SCAN has the options to set the sampling rate and the FFT size, as well as FFT window. This can be done using **Settings** panel on the left to the screen.

61

LF frequency response of the structure can be obtained using ambient struural vibrations, impact excitation of the structure, external shaker, or utilizing FN-Scan generator using tab **Generators** on the left panel. This tab allows for setting LF generator amplitude, Start Frequency, Frequency Step, and Number of steps. If this option is chosen, only Peak averaging is allowed, so the frequency response can be captured as the generator is step-sweeping through the frequency range. The generator is activated by clinking on button ▭Start located at the left top of the screen.

3.2.3. N-Scan Testing Mode

N-Scan testing mode is the original testing mode is used then external low frequency excitation is available and can be controlled by the FN-Scan system. Typically, it is used in the laboratory settings.
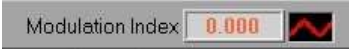
The N-Scan testing mode is set in **Settings** panel and is activated by pressing soft button ▭OK and than button ▭Start at the left top of the Screen.

The N-Scan testing mode operates as following:

- The generated ultrasonic signal is step-swept in the specified frequency range, with the specified frequency step, Δf, (the range and the step are set using Tab **Generators** (in **N-Scan Settings Panel**), so at each step, n, the frequency is changing according to $f_n = f_0 + n*\Delta f$, where n = 0, 1, 2, …N-1, N is the total number of steps set in dial box ▭ 100 .

- The low frequency vibration is set (using **Generators** setting tab) with the fixed frequency, F, (usually it is one of the resonance frequencies of the structure under test).

- The cursors are automatically set to frequencies $f_{\pm c} = f_n \pm c*F$, where c = 0, 1, 2, … C. (1+2C) is the total number of cursors, which is set in **Cursors** setting tab.

- At each frequency step, N-SCAN acquires and processes the received ultrasonic signal.[16] The signal spectrum magnitudes, $A_{\pm c}$, at cursor's frequencies, $f_{\pm c}$, are displayed on the upper portion of the Application Display as function of the frequency step, n.

- At each frequency step, N-Scan calculates the modulation indexes for each cursor. For example $M_{-1}(n) = A_{-1}/A_0$ for cursor # 2, $M_{+1}(n) = A_{+1}/A_0$ for cursor #3, etc.
- If LF Channel is used and connected to vibration sensor measuring LF vibration amplitude A_F, and the option **Normalize** is chosen in the tab **Settings** N-Scan calculates the normalized modulation indexes as $M_{-1Norm}(n) = A_{-1}/A_0A_F$, $M_{+1Norm}(n) = A_{+1}/A_0A_F$, and etc. for each cursor frequency.

- N-Scan testing mode allows for Arithmetic and Peak averaging of data at each frequency step. The averaging type and the number measurements to average at each HF frequency

is set in Tab **Average** for **HF Channel** (in **Settings**). Note, if HF Channel average is activated, LF Channel average is not allowed.

Each calculated Modulation Index is arithmetically averaged across the scanned frequency range and the results can be saved in excel file.

An averaged Modulation Index for second and first cursor's frequencies $M_{sum}(n) = \frac{1}{2}(M_{-1}(n) + M_{+1}(n))$, is also averaged across the scanned frequency range is displayed (in dB scale) at the top of the Screen as . As practice showed, this value is the most commonly used for the structural integrity evaluation and in most applications is used as a sole description of structural damage.

Nevertheless, the measurements at the other cursor frequencies could be saved as Excel files for the record keeping and post-processing.

As a rule, the Modulation Index first is determined for a control (no defect) structure to establish a baseline for the given structure. Appreciable increase of the Modulation Index (usually over 3 dB) over the established baseline indicates the presence of a defect in a structure under test: the greater the increase, the greater the defect.

If the baseline cannot be established, N-SCAN can be used for periodic or continuous monitoring: any increase in the Modulation Index during the monitoring may indicate the development and accumulation of damage.

3.2.4. FN-Scan Testing Mode

FN-Scan testing mode specifically developed for field-testing using intermittent ambient vibrations of the structure under test. In this mode, the system monitors ambient vibration using 3D accelerometer. FN-Scan operation is triggered if one of the monitored accelerometer signal exceeds the predetermined trigger level (threshold) for the predetermined time duration (all set in **Trigger** panel). The minimum threshold duration is 0.1 second and can be increase by 0.1sec increment. Once the trigger is activated, the system generates muti-sine HF ultrasonic signals, capture and store all LF and HF signal for the following processing.

In order to utilize this mode, first HF ultrasonic multi-sin signals should set in tab **AO Generator**, Fig. 3.2.4. In multi-sine window the user can set an unlimited number of sinusoidal signals with chosen frequencies, amplitude and phase. All this frequencies will be generated simultaneously for the predetermined time interval set in **Trigger** panel.

Next, the trigger level and duration as well as HF signal generation duration must be set in **Trigger** panel, Fig.3.2.5. The **TriggerArray** indicates the triggering events for the set trigger duration – each square represents 0.1 sec interval. If the trigger signal exceed its trigger level at any given 0.1 sec interval, the respective square will light up showing I real time the triggering events. The FN-Scan generation and capturing will be activated if all squares within duration

interval are lighted-up. At this point, all LF and HF signals will be captured and stored for the following up processing.
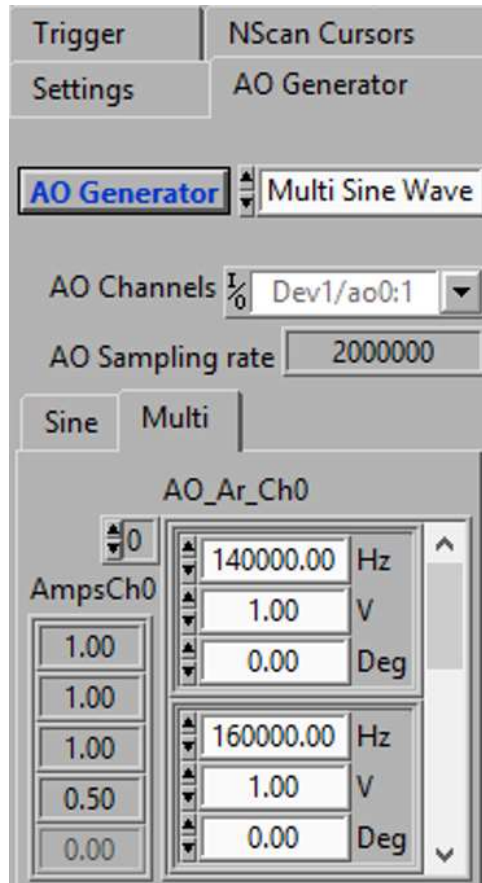

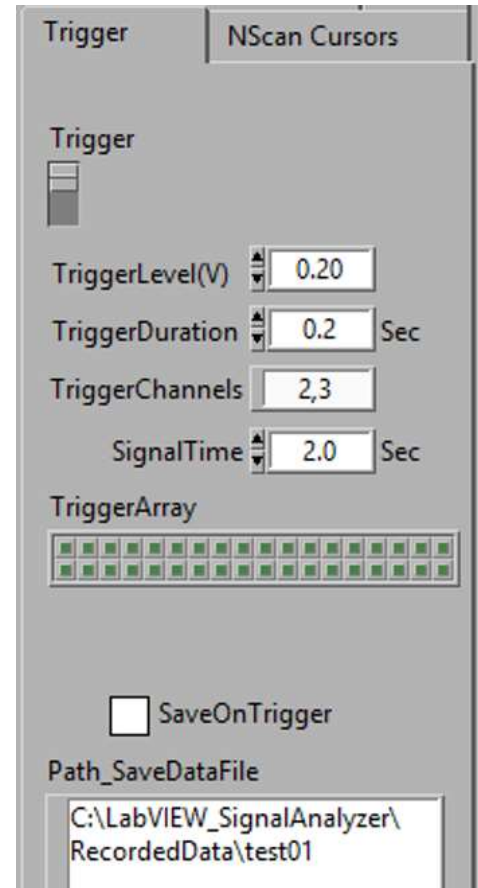Fig. 3.2.4. FN-Scan multi-sine generator setting

Fig. 3.2.5. FN-Scan trigger setting

4. SIGNAL PROCESSING AND INTERPRETATION

Presently, the processing includes calculation of averaged MI indexes in established in proven N-Scan mode. FN-Scan mode has been developed for field testing using structure ambient vibrations. There are a number of processing algorithms have been developed for this mode of operation, however these algorithms are yet to be tested and validated under the real-life field conditions. Likely, these algorithms may need some corrections and then can be programmed and integrated into the FN-Scan software. Until that, the system allow for storage of the raw data for post-processing to test/modify/validate of all of the developed algorithms.